

# Efficient Multidimensional Functional Data Analysis Using Marginal Product Basis Systems

William Consagra

Brigham and Women's Hospital, Harvard Medical School

Arun Venkataraman

Department of Physics and Astronomy, University of Rochester

Xing Qiu

Department of Biostatistics and Computational Biology, University of Rochester

September 18, 2023

## Abstract

In areas ranging from neuroimaging to climate science, advances in data storage and sensor technology have led to a proliferation in multidimensional functional datasets. A common approach to analyzing functional data is to first map the discretely observed functional samples into continuous representations, and then perform downstream statistical analysis on these smooth representations. It is well known that many of the traditional approaches used for 1D functional data representation are plagued by the curse of dimensionality and quickly become intractable as the dimension of the domain increases. In this paper, we propose a computational framework for learning continuous representations from a sample of multidimensional functional data that is immune to several manifestations of the curse. The representations are constructed using a set of separable basis functions that are defined to be optimally adapted to the data. We show that the resulting estimation problem can be solved efficiently by the tensor decomposition of a carefully defined reduction transformation of the observed data. Roughness-based regularization is incorporated using a class of differential operator-based penalties. Relevant theoretical properties are also discussed. The advantages of our method over competing methods are thoroughly demonstrated in simulations. We conclude with a real data application of our method to a clinical diffusion MRI dataset.

*Keywords:* functional data; basis representation; tensor decomposition; functional principal component analysis

# 1 Introduction

Functional data analysis (FDA) is a subfield of statistics concerned with the analysis of samples of functions. In most applications, the functional sample is not observed directly, rather, at some discrete number of domain points  $\mathbf{x}_{ij} \in \mathcal{M} \subset \mathbb{R}^D$  according to

$$Y_{ij} = U_i(\mathbf{x}_{ij}) + \epsilon_{ij}; \quad i = 1, \dots, N; j = 1, \dots, M_i$$

where  $N$  is the sample size,  $M_i$  the number of domain points for the  $i$ 'th sample,  $U_i \sim U$  is a random function and  $\epsilon_{ij}$  is additive noise. In many FDA workflows, the analyst needs to perform the initial step of estimating a smooth function  $\widehat{U}_i$  from each subject's discretely observed noisy data, i.e. the “smoothing first, then estimation” approach (Zhang and Chen, 2007), which we refer to here as *functional representation*. Various downstream analyses are then performed using these reconstructed smooth functions. In this work, we are interested in the function representation problem for *multidimensional* functional data, i.e., random functions defined on multidimensional ( $D > 1$ ) domains. Specifically, we consider the situation where the sample is observed on a common  $D$ -dimensional grid, i.e.  $\mathbf{x}_{ij}$  are the same for all subjects, a setting frequently encountered in various imaging applications.

When  $D = 1$ , functional representation can be accomplished using standard nonparametric approaches, e.g., local kernel regression or basis expansion (Ramsay and Silverman, 2005; Hsing and Eubank, 2015). For  $D > 1$ , these approaches suffer from the curse of dimensionality: the number of observations required to obtain a desired mean-squared error (Stone, 1980) and/or the number of model parameters (e.g. the number of basis functions for a tensor product basis) grow exponentially in  $D$  (Wasserman, 2010). In this scenario, semiparametric regression approaches provide a route to tractable estimation, though the associated structural assumptions are often overly restrictive for real world data. Hence, developing a general framework for multidimensional functional data analysis demands a different approach to representation.

It is well known that the optimal (minimum mean integrated squared error) low-rank representation for functional data can be formed using the eigenfunctions of the

covariance operator of the process, and thus these form an attractive basis system for parsimonious modeling. Unfortunately, estimating the eigenfunctions, i.e., performing functional principal component analysis (FPCA) (Silverman, 1996), for a general  $D$ -dimensional random function requires the nonparametric estimation of the  $2D$ -dimensional covariance function, denoted  $C(\mathbf{x}, \mathbf{y})$ . Some general techniques have recently been proposed (Chen and Jiang, 2017; Li et al., 2019; Wang et al., 2020), though the curse of dimensionality is even more problematic in this situation, due to both the dimension doubling effect and the symmetry and positive semi-definite constraints. To alleviate the computational difficulties associated with estimating a generic covariance function of a multidimensional process, a common tactic is to assume some notion of separability for  $C$  (Chen et al., 2017; Lynch and Chen, 2018). These works are mostly developed for the case when the domain naturally decomposes into a product of two spaces, e.g., space and time, though extending the theory to general  $D$ -dimensional domains is feasible. Computationally speaking, it is a different story. For instance, when  $D > 2$ , the marginal product FPCA in Chen et al. (2017) requires multidimensional numerical integration or nonparametric smoothing in order to estimate the marginal covariance functions, re-introducing a manifestation of the curse of dimensionality.

In what follows, we propose a framework for multidimensional function representation based on learning the optimal *marginal product basis* (MPB), i.e., a collection of independent multiplicatively separable functions, that avoids both direct estimation of, and explicit structural assumptions on,  $C$ . Critically, the number of parameters needed to estimate the MPB is *linear* in  $D$ , and therefore this structure is effective for combating the curse of dimensionality. We prove that the optimal MPB defines a representation space that can be considered nearly optimal for a particular rank, with an inefficiency cost that becomes negligible for large ranks. To estimate the optimal MPB from the observed data, we identify an isometric embedding which allows the reparameterization of the observed data tensor into a lower dimensional space, permitting the derivation of a fast algorithm which scales favorably with huge datasets. This is in contrast to alternative methods for optimal basis construction for multidimensional functional data which rely on a smoothed decomposition

of the raw data tensor (Huang et al., 2009; Allen, 2013; Allen and Weylandt, 2019), and as a result become computationally problematic for densely observed functions. Additionally, our approach enables a “fully functional” treatment of the estimation problem, in which the continuous basis functions are estimated directly, as opposed to the discrete factors estimated by the tensor decomposition approaches. Working directly with the continuous representations allows analytic computation of partial derivatives and inner products, thus facilitating efficient and stable two-stage algorithms for a variety of subsequent FDA tasks of interest. When working directly with the discrete data, such operations can be potentially numerically unstable (finite difference derivative approximation) or ill-defined (inner product between functions at different resolutions).

It is worth noting that the multidimensional set-up considered here has received significantly less attention than *multivariate* functional data. Multivariate FDA involves observing multiple, potentially correlated functions for each of the  $N$  samples, with most approaches focusing on the case where the domain of each univariate functional data is one-dimensional (Li et al., 2020). Approaches to analyzing *multivariate multidimensional* functional data typically first require a functional representation for each univariate multidimensional domain, which are then used for the multivariate analysis (Happ and Greven, 2018). As a result, this work can be seamlessly integrated with such methods.

The rest of the paper is organized as follows. In Section 2, we formulate the optimal MPB system and discuss relevant theoretical properties. In Section 3, we derive an efficient estimation procedure and discuss the incorporation of roughness-based regularization using differential operators as well as hyperparameter selection. In Section 4, we illustrate how to utilize the MPB to derive a fast two-stage multidimensional FPCA. Section 5 compares the proposed method with competing methods in simulation studies. In Section 6, we analyze a set of magnetic resonance imaging data from a traumatic brain injury study. Section 7 offers concluding remarks and potential future directions. Proofs for all theorems can be found in Supplemental Materials. Code for our algorithms and scripts to reproduce all of the results in the simulation section have been made publicly available in a python package: <https://github.com/Will-Consagra/eMFDA>.

## 2 Marginal Product Models

### 2.1 Background and Model Description

Let  $U$  be a multidimensional random function with real-valued square integrable realizations, i.e.  $U_i \sim U \in \mathcal{H} := \mathbb{L}^2(\mathcal{M})$ . We assume the domain can be decomposed as  $\mathcal{M} = \mathcal{M}_1 \times \cdots \times \mathcal{M}_D$ , so for  $\mathbf{x} = (x_1, \dots, x_D)' \in \mathcal{M}$ ; each  $x_d$ , for  $d = 1, \dots, D$ , is a member in the marginal domain  $\mathcal{M}_d$ , which is assumed to be a compact subset of Euclidean space  $\mathbb{R}^{p_d}$ . Without loss of generality, we assume the Lebesgue measure of  $\mathcal{M}$  is 1. We make the following regularity assumptions on  $U$ :

*Assumption 1.* (a)  $\mathbb{E}[U] = 0$ , (b)  $\mathbb{E}[\int_{\mathcal{M}} U^2(\mathbf{x})d\mathbf{x}] < \infty$ , and (c)  $U$  is *mean-square continuous*.

The mean zero assumption on  $U$  is made for convenience of presentation, and the mean square integrability and mean-square continuity assumptions are a standard requirement (Hsing and Eubank, 2015). Under Assumption 1, we are guaranteed that the covariance function  $C(\mathbf{x}, \mathbf{y}) := \mathbb{E}[U(\mathbf{x})U(\mathbf{y})]$  is continuous on  $\mathcal{M} \times \mathcal{M}$ . By Mercer's theorem, this covariance function has an eigen-decomposition  $C(\mathbf{x}, \mathbf{y}) = \sum_{k=1}^{\infty} \rho_k \psi_k(\mathbf{x})\psi_k(\mathbf{y})$ , where  $\{\psi_k\}_{k=1}^{\infty}$  forms a complete orthonormal sequence of eigenfunctions in  $\mathcal{H}$  and  $\{\rho_k\}_{k=1}^{\infty}$  is a non-increasing sequence of real, non-negative eigenvalues. Additionally, by the Karhunen-Loève theorem, with probability one we have the decomposition  $U(\mathbf{x}) = \sum_{k=1}^{\infty} Z_k \psi_k(\mathbf{x})$ , where  $Z_k = \langle U, \psi_k \rangle_{\mathcal{H}}$ , which are mean zero random variables with  $\mathbb{E}[Z_k Z_j] = \rho_k \mathbb{I}\{k = j\}$ .

Let  $H_d := \mathbb{L}^2(\mathcal{M}_d)$ , so that  $\mathcal{H} := \mathbb{L}^2(\mathcal{M}) = \bigotimes_{d=1}^D H_d$ , the tensor product of  $D$  member spaces. We assume that there exists a complete basis system,  $\boldsymbol{\phi}_d := \{\phi_{d,j}\}_{j=1}^{\infty}$ , for each marginal function space  $H_d$ . Denote their rank- $m_d$  truncations as  $\boldsymbol{\phi}_{m_d,d} = (\phi_{d,1}, \dots, \phi_{d,m_d})'$ ;  $H_{m_d,d} := \text{span}(\boldsymbol{\phi}_{m_d,d})$ ; and  $\mathcal{H}_{\mathbf{m}} := \bigotimes_{d=1}^D H_{m_d,d}$ , where  $\mathbf{m} = (m_1, \dots, m_D)'$  are the marginal ranks. By construction,

$$\boldsymbol{\tau}_{\mathbf{m}} := \bigotimes_{d=1}^D \boldsymbol{\phi}_{m_d,d} = \left\{ \tau_{j_1, \dots, j_D}(\mathbf{x}) = \prod_{d=1}^D \phi_{d,j_d}(x_d), j_d = 1, \dots, m_d \right\}$$

is the complete tensor product bases (TPB) for  $\mathcal{H}_{\mathbf{m}}$ .

**Definition 2.1** (Marginal product structure).  $\zeta \in \mathcal{H}$  is called a rank-1 marginal product function if it is *multiplicatively separable*, and  $u \in \mathcal{H}$  is called a rank- $K$  marginal product

function if it is a linear combination of  $K$  independent rank-1 marginal product functions:

$$u(\mathbf{x}) = \sum_{k=1}^K b_k \zeta_k(\mathbf{x}) = \sum_{k=1}^K b_k \prod_{d=1}^D \xi_{k,d}(x_d), \quad \xi_{k,d} \in H_d, \quad b_k \in \mathbb{R}. \quad (1)$$

We denote the collection of rank-1 marginal product functions with marginal ranks  $\mathbf{m}$ :

$$\mathcal{L}_{\mathbf{m}} := \left\{ \zeta(\mathbf{x}) : \zeta(\mathbf{x}) = \prod_{d=1}^D \xi_d(x_d), \xi_d \in H_{m_d,d}, \|\xi_d\|_{H_d} = 1 \right\} \quad (2)$$

In this work, we propose to estimate the optimal basis set of  $K$  elements from  $\mathcal{L}_{\mathbf{m}}$  for representing realizations of  $U$ , a notion formalized as follows:

**Definition 2.2** (Optimal Rank- $K$  MPB). Define the set of functions

$$\mathcal{V}_{K,\mathbf{m}} := \left\{ \zeta = (\zeta_1, \dots, \zeta_K)' : \zeta_k \in \mathcal{L}_{\mathbf{m}}, \zeta_1, \dots, \zeta_K \text{ linearly independent} \right\}, \quad (3)$$

and define the associated optimal rank  $K$  MPB, denoted  $K$ -oMPB, as

$$\zeta_{\mathbf{m}}^* = \arg \inf_{\zeta \in \mathcal{V}_{K,\mathbf{m}}} \mathbb{E} \left\| U - P_{\zeta}(U) \right\|_{\mathcal{H}}^2. \quad (4)$$

where  $P_{\zeta}$  is the projection operator onto  $\text{span}(\zeta)$ .

Given a random sample of  $N$  realizations  $U_i \sim U$ , define the corresponding empirical estimate of (4) as

$$\check{\zeta}_{\mathbf{m},N}^* = \arg \inf_{\zeta \in \mathcal{V}_{K,\mathbf{m}}} \frac{1}{N} \sum_{i=1}^N \left\| U_i - P_{\zeta}(U_i) \right\|_{\mathcal{H}}^2 \quad (5)$$

## 2.2 Approximation Properties

We now characterize the expected asymptotic approximation power of  $\check{\zeta}_{\mathbf{m},N}^*$ . Let  $\mathcal{A}_k$  be the  $D$ -mode tensor with elements  $\mathcal{A}_k(j_1, \dots, j_D)$  defined by

$$P_{\mathcal{H}_m}(\psi_k) = \sum_{j_1=1}^{m_1} \cdots \sum_{j_D=1}^{m_D} \mathcal{A}_k(j_1, \dots, j_D) \phi_{1,j_1} \cdots \phi_{D,j_D},$$

where  $P_{\mathcal{H}_m}$  is the projection operator onto  $\mathcal{H}_m$ . Denote  $\mathcal{A}^{(K)}$  as the tensor obtained by the  $D+1$  mode stacking of  $\mathcal{A}_1, \dots, \mathcal{A}_K$ . Let  $\mathbf{J}_{\phi_d} \in \mathbb{R}^{m_d \times m_d}$  be the matrix of pairwise  $\mathcal{H}_{m_d,d}$  inner products of  $\phi_{m_d,d}$ . Define the inner-product space  $(\otimes_{d=1}^D \mathbb{R}^{m_d} \otimes \mathbb{R}^K, \langle \cdot, \cdot \rangle_{\tilde{F},C})$  where

$$\langle \mathcal{T}_1, \mathcal{T}_2 \rangle_{\tilde{F},C} = \sum_{k=1}^K \rho_k \langle \mathcal{T}_1(:, \dots, :, k), \mathcal{T}_2(:, \dots, :, k) \times_1 \mathbf{J}_{\phi_1} \cdots \times_D \mathbf{J}_{\phi_D} \rangle_F$$

for tensors  $\mathcal{T}_1, \mathcal{T}_2 \in \otimes_{d=1}^D \mathbb{R}^{m_d} \otimes \mathbb{R}^K$ , where  $\times_d$  denotes the tensor  $d$ -mode multiplication.

**Theorem 2.1** (Generalization Error). *With slight abuse of notation, denote  $P_{\check{\zeta}_{\mathbf{m},N}^*}$  as the projection operator onto  $\text{span}(\check{\zeta}_{\mathbf{m},N}^*)$  and let the function  $w_{\tau_{\mathbf{m}}}(\mathbf{m})$  be the  $\mathbb{L}^2(\mathcal{M})$  convergence rate of the TPB system  $\tau_{\mathbf{m}}$  (Definition S1.1 in the supplemental materials). Under Assumptions 1 and S2, S3 in the supplementary material,*

$$\mathbb{E} \left\| U - P_{\check{\zeta}_{\mathbf{m},N}^*}(U) \right\|_{\mathcal{H}}^2 \leq \sum_{k=K+1}^{\infty} \rho_k + \left\| \mathcal{A}^{(K)} - \widehat{\mathcal{A}}_K^{(K)} \right\|_{\bar{F},C}^2 + O(w_{\tau_{\mathbf{m}}}(\mathbf{m})) + O_p(N^{-1/2}) \quad (6)$$

where the expectation is taken with respect to a new realization of  $U$  and  $\widehat{\mathcal{A}}_K^{(K)}$  is the rank  $K$  canonical polyadic decomposition of the coefficient tensor  $\mathcal{A}^{(K)}$  under the  $\|\cdot\|_{\bar{F},C}$ -norm.

Theorem 2.1 bounds the expected generalization error of  $\check{\zeta}_{\mathbf{m},N}^*$  by the sum of four terms. The first term is the tail sum of the eigenvalues, which is the expected generalization error of the optimal rank  $K$  basis system (the eigenfunctions). The third term is the irreducible bias from the finite truncation of the marginal ranks  $\mathbf{m}$ . The fourth term reflects the finite sample statistical approximation error and can be established using convergence results from the theory of M-estimators. The second term shows that the inefficiency cost incurred by representing the function realizations with  $\check{\zeta}_{\mathbf{m},N}^*$ , as opposed to the eigenfunctions, is driven by the low-rank structure of  $\mathcal{A}^{(K)}$ . This term is unknown in practice but vanishes for large enough  $K$  (often,  $K \ll \prod_{d=1}^D m_d$ ) though this value will depend on the particular tensor product space  $\tau$ , marginal ranks  $\mathbf{m}$  and covariance function  $C$ . Please visit Section S1 of the Supplemental Materials for further technical discussion on these and related theoretical matters. We now turn our attention to the development of computationally efficient algorithms to estimate  $\check{\zeta}_{\mathbf{m},N}^*$  in practice.

## 3 Estimation

### 3.1 Discrete Observation Model

We consider the case in which the  $U_i$  are observed with noise at each discrete location of a multidimensional grid  $\mathcal{X} \subset \mathcal{M}$ , where

$$\mathcal{X} = (x_{11}, x_{12}, \dots, x_{1n_1})' \times (x_{21}, x_{22}, \dots, x_{2n_2})' \times \cdots \times (x_{D1}, x_{D2}, \dots, x_{Dn_D})',$$

and each vector of marginal grid points  $\mathbf{x}_d := (x_{d1}, x_{d2}, \dots, x_{dn_d}) \in \mathcal{M}_d$ , according to the canonical observation model

$$\mathcal{Y}(i_1, i_2, \dots, i_D, i) = U_i(x_{1,i_1}, x_{2,i_2}, \dots, x_{D,i_D}) + \mathcal{E}(i_1, i_2, \dots, i_D, i) \quad (7)$$

for  $i_d = 1, 2, \dots, n_d$ ,  $d = 1, 2, \dots, D$ ,  $i = 1, 2, \dots, N$ , where  $\mathcal{Y}$  is a  $D + 1$ -mode tensor with dimensions  $(n_1, n_2, \dots, n_D, N)$ ,  $\mathbb{E}[\text{vec}(\mathcal{E})] = \mathbf{0}$  and  $\text{Var}[\text{vec}(\mathcal{E})] = \sigma^2 \mathbf{I}$ . The discretized counterpart to (5) is given by

$$\widehat{\zeta}_{N,m}^* := \arg \inf_{\zeta \in \mathcal{V}_{K,m}} \min_{\mathbf{B} \in \mathbb{R}^{N \times K}} \frac{1}{N} \sum_{i=1}^N \left\| \mathcal{Y}_i - \sum_{k=1}^K \mathbf{B}_{i,k} \bigotimes_{d=1}^D \boldsymbol{\xi}_{d,k} \right\|_F^2. \quad (8)$$

where  $\mathcal{Y}_i \in \mathbb{R}^{n_1 \times \dots \times n_D}$  is the observed data tensor for the  $i$ th realization,  $\boldsymbol{\xi}_{d,k} \in \mathbb{R}^{n_d}$  is the evaluation of  $\xi_{k,d}$  on  $\mathbf{x}_d$  and  $\mathbf{B}$  is the matrix of coefficients for the  $\zeta_k$ 's for each of the  $N$  samples.

### 3.2 A Convenient Reparameterization

First we note that for  $\zeta \in \mathcal{V}_{K,m}$ , we have the representation  $\xi_{k,d}(x_d) = \sum_{j=1}^{m_d} c_{d,k,j} \phi_{d,j}(x_d)$ . Consequently  $\widehat{\zeta}_{N,m}^*$  is equivalently defined by the solutions to the following optimization problem

$$(\widehat{\mathbf{C}}_1, \dots, \widehat{\mathbf{C}}_D) := \arg \inf_{(\mathbf{C}_1, \dots, \mathbf{C}_D)} \min_{\mathbf{B}} \frac{1}{N} \sum_{i=1}^N \left\| \mathcal{Y}_i - \sum_{k=1}^K \mathbf{B}_{i,k} \bigotimes_{d=1}^D \boldsymbol{\Phi}_d \mathbf{c}_{d,k} \right\|_F^2 \quad (9)$$

where  $\boldsymbol{\Phi}_d \in \mathbb{R}^{n_d \times m_d}$  is the evaluation of  $\phi_{m_d,d}$  on the marginal grid  $\mathbf{x}_d$ , i.e.  $\boldsymbol{\Phi}_{d,i_d j_d} := \phi_{d,j_d}(x_{d,i_d})$ ,  $\mathbf{c}_{d,k} \in \mathbb{R}^{m_d}$  is the coefficient of  $\xi_{k,d}$ , and  $\mathbf{C}_d$  is the matrix whose columns are the  $\mathbf{c}_{d,k}$ . Note that the unit  $\|\cdot\|_{H_d}$  norm constraint in the definition of  $\mathcal{V}_{K,m}$  is translated to a norm constraint on the columns of the  $\mathbf{C}_d$ 's that must be incorporated for identifiability reasons. For clarity of presentation, we defer additional discussion of this and related identifiability matters to Section S1 of the supplemental materials.

Denote the SVD of the basis evaluation matrices  $\boldsymbol{\Phi}_d = \mathbf{U}_d \mathbf{D}_d \mathbf{V}_d'$ . In general, we have  $n_d > m_d$ , so  $\mathbf{U}_d \in \mathbb{R}^{n_d \times m_d}$  is a semi-orthogonal matrix;  $\mathbf{D}_d \in \mathbb{R}^{m_d \times m_d}$  is an invertible diagonal matrix; and  $\mathbf{V}_d \in \mathbb{R}^{m_d \times m_d}$  is an orthogonal matrix. For any  $\zeta \in \mathcal{V}_{K,m}$ , the evaluation of the MPB functions  $\boldsymbol{\xi}_d = (\xi_{d1}, \dots, \xi_{dK})'$  on  $\mathbf{x}_d$ , is represented as

$$\boldsymbol{\Xi}_d = \boldsymbol{\Phi}_d \mathbf{C}_d = \mathbf{U}_d \mathbf{D}_d \mathbf{V}_d' \mathbf{C}_d = \mathbf{U}_d \widetilde{\mathbf{C}}_d, \quad \widetilde{\mathbf{C}}_d := \mathbf{D}_d \mathbf{V}_d' \mathbf{C}_d.$$



The following theorem proves the equivalence between the solution of Equation (9) and the rank- $K$  canonical polyadic decomposition (CPD) of an appropriately defined transformation of the observed data tensor  $\mathcal{Y}$ .

**Theorem 3.1** (Functional Tensor Decomposition Theorem). *Define  $\widehat{\mathcal{G}} := \mathcal{Y} \times_1 \mathbf{U}'_1 \times_2 \mathbf{U}'_2 \cdots \times_D \mathbf{U}'_D$ , which is a  $(D + 1)$ -mode tensor with dimensions  $(m_1, m_2, \dots, m_D, N)$ , and denote its rank- $K$  decomposition by  $\widehat{\mathcal{G}}_K(\mathbf{B}, \tilde{\mathbf{C}}) = \sum_{k=1}^K \left[ \bigotimes_{d=1}^D \tilde{\mathbf{c}}_{d,k} \right] \otimes \mathbf{b}_k$ , with factor matrices  $\mathbf{B} \in \mathbb{R}^{N \times K}$  and  $\tilde{\mathbf{C}} = [\tilde{\mathbf{C}}_1, \dots, \tilde{\mathbf{C}}_D]$ ,  $\tilde{\mathbf{C}}_d \in \mathbb{R}^{m_d \times K}$ .  $\tilde{\mathbf{c}}_{d,k}$  and  $\mathbf{b}_k$  are the  $k$ th column of  $\tilde{\mathbf{C}}_d$  and  $\mathbf{B}$ , respectively. The optimization problem (9) has the following solutions:  $\widehat{\mathbf{B}} = \mathbf{B}$  and  $\widehat{\mathbf{C}}_d = \mathbf{V}_d \mathbf{D}_d^{-1} \tilde{\mathbf{C}}_d$ , for  $d = 1, \dots, D$ .*

Theorem 3.1 reveals that estimating the  $K$ -oMPB is equivalent to the CPD of the compressed  $\widehat{\mathcal{G}}$  tensor. As the dimensionality of  $\widehat{\mathcal{G}}$  is controlled by the marginal ranks  $m_d$ , as opposed to the number of marginal grid points  $n_d$ , this defines a practical reduction transformation which permits user control of the dimensionality of the optimization problem.

### 3.3 Regularization in the Transformed Space

In order to ameliorate the influence of noise and discretization and to promote smoothness in the estimated  $K$ -oMPB basis, we incorporate a regularization term to the objective function in Equation (9) of the form:

$$\sum_{k=1}^K \text{Pen}(\zeta_k) = \sum_{k=1}^K \int_{\mathcal{M}} \sum_{d=1}^D \lambda_d L_d^2(\xi_{k,d})$$

for some  $\lambda_d > 0$ , where  $L_d : \mathbb{W}^{\alpha_d, 2}(\mathcal{M}_d) \rightarrow \mathbb{L}^2(\mathcal{M}_d)$  is a linear (partial) differential operator, and  $\mathbb{W}^{\alpha_d, 2}(\mathcal{M}_d)$  is the Sobolev space over the  $d$ th marginal domain, with order  $\alpha_d$  defined appropriately.

**Proposition 3.2.** *Let  $\mathbf{T}_d := \mathbf{D}_d^{-1} \mathbf{V}'_d \mathbf{R}_d \mathbf{V}_d \mathbf{D}_d^{-1}$ , with  $\mathbf{R}_d(i, j) = \int_{\mathcal{M}_d} L_d(\phi_{d,i}) L_d(\phi_{d,j})$ , then  $\sum_{k=1}^K \text{Pen}(\zeta_k) = \sum_{d=1}^D \lambda_d \text{tr}(\tilde{\mathbf{C}}'_d \mathbf{T}_d \tilde{\mathbf{C}}_d)$ .*

As a consequence, such penalties are quadratic in the transformed coordinate matrices  $\tilde{\mathbf{C}}_d$  and therefore convex. This permits the derivation of efficient numerical algorithms to estimate the optimal MPB functions, which will be discussed in Section 3.4.

Penalization of the coefficient matrix  $\mathbf{B}$  is incorporated using the penalty function denoted  $l(\mathbf{B})$ . We assume that  $l(\mathbf{B})$  is convex, which is a requirement to guarantee the convergence of the algorithm in Section 3.4, but otherwise leave its form unspecified. For example, lasso-type penalties can be integrated to promote sparsity in the MPB functional representation for interpretability or feature extraction. Using the results from Theorem 3.1 and Proposition 3.2, the solution to the regularized augmentation of Equation (9) is a linear transformation of the solution to

$$\arg \min_{\tilde{\mathbf{C}}_1, \dots, \tilde{\mathbf{C}}_D, \mathbf{B}} \left\| \hat{\mathbf{G}} - \sum_{k=1}^K \bigotimes_{d=1}^D \tilde{\mathbf{c}}_{d,k} \otimes \mathbf{b}_k \right\|_F^2 + \sum_{d=1}^D \lambda_d \text{tr}(\tilde{\mathbf{C}}_d' \mathbf{T}_d \tilde{\mathbf{C}}_d) + \lambda_{D+1} l(\mathbf{B}). \quad (10)$$

### 3.4 Algorithm

In general, it can be shown that the optimization problem (10) is non-convex and NP-hard (Hillar and Lim, 2013). To derive a computationally tractable approximation algorithm, we propose a block coordinate descent based approach in which, for the  $(r+1)$ 'th iteration, the variables are updated according to the sequence of conditional minimization problems

$$\tilde{\mathbf{C}}_d^{(r+1)} = \min_{\mathbf{X}} g(\tilde{\mathbf{C}}_1^{(r+1)}, \dots, \tilde{\mathbf{C}}_{d-1}^{(r+1)}, \mathbf{X}, \tilde{\mathbf{C}}_{d+1}^{(r)}, \dots, \tilde{\mathbf{C}}_D^{(r)}, \mathbf{B}^{(r)}), \quad (11)$$

for  $d = 1, \dots, D$  and likewise for  $\mathbf{B}^{(r+1)}$ , where  $g$  denotes the objective function from (10).

Using the properties of the  $d$ -mode matricization, we can write the conditional minimization problem defining the update of  $\tilde{\mathbf{C}}_d$  as

$$\tilde{\mathbf{C}}_d^{(r+1)} = \min_{\tilde{\mathbf{C}}_d} \|\mathbf{G}'_{(d)} - \tilde{\mathbf{C}}_d \mathbf{W}_d^{(r)'}\|_F^2 + \lambda_d \text{tr}(\tilde{\mathbf{C}}_d' \mathbf{T}_d \tilde{\mathbf{C}}_d). \quad (12)$$

The update for  $\mathbf{B}$  is given by

$$\mathbf{B}^{(r+1)} = \min_{\mathbf{B}} \|\mathbf{G}_{(D+1)} - \mathbf{W}_{D+1}^{(r)} \mathbf{B}'\|_F^2 + \lambda_{D+1} l(\mathbf{B}), \quad (13)$$

where  $\mathbf{W}_d^{(r)} = (\odot_{j < d}^D \tilde{\mathbf{C}}_j^{(r+1)} \odot_{j > d}^D \tilde{\mathbf{C}}_j^{(r)}) \odot \mathbf{B}^{(r)}$  for  $d = 1, \dots, D$ ,  $\mathbf{W}_{D+1}^{(r)} = \odot_{d=1}^D \tilde{\mathbf{C}}_d^{(r+1)}$  and  $\mathbf{G}_{(d)}$  is the  $d$ -mode unfolding of tensor  $\hat{\mathbf{G}}$ . Here  $\odot$  is the Khatri–Rao product. From here on the superscript  $r$  denoting iteration is dropped for clarity.

In fact, the solution to the subproblem (12) is equivalent to the solution to

$$\tilde{\mathbf{C}}_d \mathbf{W}_d' \mathbf{W}_d + \lambda_d \mathbf{T}_d \tilde{\mathbf{C}}_d = \mathbf{W}_d' \mathbf{G}_{(d)}. \quad (14)$$

This equivalence can be verified by noting that (14) defines the gradient equations of (12) and that the solution is globally optimum due to convexity. Equation (14) is known as the Sylvester equation and has a unique solution under very mild conditions (specifically  $\mathbf{W}'_d \mathbf{W}_d$  and  $\lambda_d \mathbf{T}_d$  must have no common eigenvalues). Efficient algorithms for solving the Sylvester equation (Bartels and Stewart, 1972) are readily available in most common numerical computing languages.

Notice that by introducing the auxiliary variable  $\mathbf{Z} = \mathbf{B}'$ , the subproblem (13) can be written in separable form as

$$\begin{aligned} \min_{\mathbf{B}, \mathbf{Z}} \quad & \|\mathbf{G}_{(D+1)} - \mathbf{W}_{D+1} \mathbf{Z}\|_F^2 + \lambda_{D+1} l(\mathbf{B}) \\ \text{subject to} \quad & \mathbf{B} - \mathbf{Z}' = \mathbf{0}. \end{aligned} \tag{15}$$

A numerical approximation to problems of the form (15) can be found using an alternating direction method of multipliers (ADMM) algorithm (Boyd et al., 2011). The ADMM scheme consists of the iterates

$$\mathbf{B}_{\text{update}} \leftarrow \min_{\mathbf{B}} (\lambda_{D+1} l(\mathbf{B}) + \gamma \|\mathbf{B} - \mathbf{Z}' + \mathbf{A}^*\|_F^2) \tag{16}$$

$$\mathbf{Z}_{\text{update}} \leftarrow \min_{\mathbf{Z}} (\|\mathbf{G}_{(D+1)} - \mathbf{W}_{D+1} \mathbf{Z}\|_F^2 + \gamma \|\mathbf{B} - \mathbf{Z}' + \mathbf{A}^*\|_F^2) \tag{17}$$

$$\mathbf{A}^*_{\text{update}} \leftarrow \mathbf{A}^* + \mathbf{B} - \mathbf{Z}' \tag{18}$$

for some choice of  $\gamma > 0$ , where  $\mathbf{A}^*$  is the scaled dual variable associated with the constraint. Since  $l$  is assumed to be convex, the ADMM iterates are guaranteed to converge.

The update (17) is a matrix ridge regression and has analytic solution given by

$$\mathbf{Z}_{\text{update}} = [\mathbf{W}'_{D+1} \mathbf{W}_{D+1} + \gamma \mathbf{I}]^{-1} [\mathbf{W}'_{D+1} \mathbf{G}_{(D+1)} + \gamma (\mathbf{B} + \mathbf{A}^*)]. \tag{19}$$

The update (16) defines the so-called *proximal operator* of  $l$  and is uniquely minimized. The exact solution will depend on the form of  $l$ , but it can be shown that many reasonable choices permit an analytic result. For example, if  $l(\cdot) = \|\cdot\|_1$ , the update is given by the element-wise soft thresholding operator applied to matrix  $\mathbf{Z}' - \mathbf{A}^*$ .

Algorithm 1 in the Supplemental Material provides pseudocode for estimating the  $K$ -oMPB utilizing the block coordinate descent scheme, referred to from here on as MARGARITA

(MARGinal-product bASis Representation with Tensor Analysis). The convergence of MARGARITA to a stationary point can be guaranteed if each of the sub-problems is convex and has a unique solution (Bertsekas, 1997). The former property is satisfied by our construction, while the latter is difficult to verify in practice but can be enforced with minor augmentations. In particular, adding an additional proximal regularization of the form  $\frac{\mu_d^{(r)}}{2} \left\| \mathbf{X} - \tilde{\mathbf{C}}_d^{(r)} \right\|_F^2$ , for  $\mu_d^{(r)} > 0$  to (11) guarantees strong convexity, and hence convergence.

We conclude this section with several remarks on practical implementation. Forming the matrix products  $\mathbf{W}'_d \mathbf{W}_d$  and  $\mathbf{W}'_d \mathbf{G}_{(d)}$  can become computationally expensive when  $D$  and/or  $m_d$  become sufficiently large. To avoid this computational bottleneck, the former can be calculated efficiently by leveraging the identity  $[\odot_i A_i]' [\odot_i A_i] = \circ_i A_i' A_i$ , where  $\circ$  is the Hadamard product. Algorithms for efficient computation of the latter have been developed, see Phan et al. (2013). Following the suggestion of Huang et al. (2016), we found success setting  $\gamma = \|\mathbf{W}'_{D+1} \mathbf{W}_{D+1}\|_F / K$ . Finally, if  $l(\cdot) = \|\cdot\|_F^2$ , then it is easy to show that (13) has a closed form solution and thus the ADMM scheme need not be invoked for this special case.

### 3.5 Hyperparameter Selection

A distinct advantage of our methodology is its flexibility in allowing the user to incorporate different notions of smoothness, via linear differential operator  $L_d$ , different choices of marginal basis systems and alternative coefficient penalty methods. In some cases, these can be selected using a-priori knowledge of the problem of interest, though for many applications a data-driven approach to hyperparameter selection may be of interest or of necessity. While our method provides the flexibility of setting  $\lambda_d$  independently for all  $d = 1, \dots, D + 1$ , using a data-driven method to select all these parameters is computationally infeasible for even moderately large  $D$ . Therefore, absent a-priori knowledge of different behavior in different dimensions, we suggest setting  $\lambda_d = \lambda_f$  for  $d = 1, \dots, D$  and selecting the parameters  $(\lambda_f, \lambda_{D+1})'$  by minimizing the  $n$ -fold cross-validation error over a 2-dimensional grid. Pseudocode for this scheme is provided in Algorithm 2 in the Supplemental Materials. Our method also requires the specification of both marginal ranks  $\mathbf{m}$  and a global rank  $K$ .

We propose the following two proportion of variance explained measures

$$PVG(K) = \|\mathcal{G} - \sum_{k=1}^K \mathbf{b}_k \otimes (\bigotimes_{d=1}^D \tilde{\mathbf{c}}_{d,k})\|_F^2 / \|\mathcal{G}\|_F^2, \quad \text{PVM}(\mathbf{m}) := \|\mathcal{Y} \times_{d=1}^D \mathbf{U}'_d\|_F^2 / \|\mathcal{Y}\|_F^2,$$

which can be used along with an elbow type criteria for selection. A detailed elaboration, justification and numerical evaluation for the proposed hyperparameter selection criteria is provided in Section S3 of the supplemental text.

## 4 Multidimensional Penalized FPCA

In this section, we demonstrate how to leverage the MPB structure to define a fast multidimensional FPCA which avoids the curse of dimensionality, incurring only trivial additional computational expense beyond MARGARITA. Consider the method for FPCA proposed in Silverman (1996), in which the  $j$ th eigenfunction  $\psi_j$  is defined as the function maximizing the penalized sample variance with modified orthogonality constraints

$$\hat{\psi}_j = \max_{\psi \in \mathbb{W}^{\alpha,2}(\mathcal{M})} \frac{\sum_{i=1}^N \text{Var}(\langle \psi, U_i \rangle_{\mathcal{H}})}{\langle \psi, \psi \rangle_{\lambda}} \quad (20)$$

s.t.  $\|\psi\|_{\mathcal{H}}^2 = 1, \quad \langle \psi, \psi_k \rangle_{\lambda} = 0, \text{ for } k = 1, 2, \dots, j-1.$

Here  $\langle \psi, \psi_k \rangle_{\lambda} := \langle \psi, \psi_k \rangle_{\mathcal{H}} + \lambda \langle L(\psi_j), L(\psi_k) \rangle_{\mathcal{H}}$  and  $L : \mathbb{W}^{\alpha,2}(\mathcal{M}) \rightarrow \mathcal{H}$  is an  $\alpha$ 'th order linear differential operator quantifying the global roughness. For simplicity, hereafter we define  $L := \Delta_{\mathcal{M}}$ , the Laplacian operator on  $\mathcal{M}$ , though other linear differential operators can be incorporated effortlessly. In our set-up,  $L$  facilitates the optional incorporation of a flexible global notion of smoothness in addition to the marginally independent regularization in Equation (10), e.g. penalizing mixed partial derivatives.

In the 1-dimensional case, the optimization problem (20) is solved using a two-stage approach: first computing  $\widehat{U}_i$  through expansion over some suitable basis system and then looking for solutions  $\hat{\psi}_j$  in the span of that set of basis functions. Analogously, we can first represent the realizations with the  $K$ -oMPB:  $\widehat{U}_i(\mathbf{x}) = \mathbf{b}'_i \boldsymbol{\zeta}_m^*(\mathbf{x})$ , and then solve Equation (20) with the additional constraint  $\psi_j \in \text{span}(\boldsymbol{\zeta}_m^*)$ , i.e.  $\psi_j(\mathbf{x}) = \mathbf{s}'_j \boldsymbol{\zeta}_m^*(\mathbf{x})$  for

some  $\mathbf{s}_j \in \mathbb{R}^K$ . Under this setup, the optimization problem (20) is equivalent to

$$\mathbf{s}_j = \max_{\mathbf{s}} \frac{\mathbf{s}' \mathbf{J}_{\zeta_m^*} \Sigma_{\mathbf{b}} \mathbf{J}_{\zeta_m^*} \mathbf{s}}{\mathbf{s}' \mathbf{J}_{\zeta_m^*} \mathbf{s} + \lambda \mathbf{s}' \mathbf{R}_{\zeta_m^*} \mathbf{s}} \quad (21)$$

$$\text{s.t. } \mathbf{s}' \mathbf{J}_{\zeta_m^*} \mathbf{s} = 1, \quad \mathbf{s}' [\mathbf{J}_{\zeta_m^*} + \lambda \mathbf{R}_{\zeta_m^*}] \mathbf{s}_k = 0, \text{ for } k = 1, 2, \dots, j-1.$$

Here  $\Sigma_{\mathbf{b}} = \text{Cov}(\mathbf{b})$  and  $\mathbf{J}_{\zeta_m^*}$ ,  $\mathbf{R}_{\zeta_m^*}$  are symmetric PSD matrices with elements  $[\mathbf{J}_{\zeta_m^*}]_{ij} = \langle \zeta_i^*, \zeta_j^* \rangle_{\mathcal{H}}$  and  $[\mathbf{R}_{\zeta_m^*}]_{ij} = \langle \Delta_{\mathcal{M}}(\zeta_i^*), \Delta_{\mathcal{M}}(\zeta_j^*) \rangle_{\mathcal{H}}$ , respectively. The objective function in Equation (21) is a generalized Rayleigh quotient and it can be shown that the solutions for  $j = 1, \dots, K^\ddagger$  are equivalently defined by the first  $K^\ddagger$  solutions to the generalized eigenvalue problem

$$\mathbf{J}_{\zeta_m^*} \Sigma_{\mathbf{b}} \mathbf{J}_{\zeta_m^*} \mathbf{s}_j = \nu_j [\mathbf{J}_{\zeta_m^*} + \lambda \mathbf{R}_{\zeta_m^*}] \mathbf{s}_j, \quad (22)$$

hence, the vector of estimated eigenfunctions is  $\hat{\boldsymbol{\psi}}(\mathbf{x}) := (\mathbf{s}'_1 \zeta_m^*(\mathbf{x}), \dots, \mathbf{s}'_{K^\ddagger} \zeta_m^*(\mathbf{x}))'$ .

There are a variety of algorithms to solve the generalized eigenvalue problem (22). In practice, we use Algorithm 9.4.2 in Ramsay and Silverman (2005), which requires the computation of the marginal inner product matrices:  $\mathbf{J}_{\phi_d}(i, j) = \langle \phi_{d,i}, \phi_{d,j} \rangle_{\mathcal{H}_d}$ ,  $\mathbf{R}_{\phi_d}(i, j) = \langle \Delta_{\mathcal{M}_d}(\phi_{d,i}), \Delta_{\mathcal{M}_d}(\phi_{d,j}) \rangle_{\mathcal{H}_d}$ , and  $\mathbf{E}_{\phi_d}(i, j) = \langle \phi_{d,i}, \Delta_{\mathcal{M}_d}(\phi_{d,j}) \rangle_{\mathcal{H}_d}$ . Given the  $\mathbf{C}_d$ 's, simple derivations show that the marginal product structure of the  $\zeta_k$ 's permits fast analytic computation of  $\mathbf{J}_{\zeta_m^*}$  and  $\mathbf{R}_{\zeta_m^*}$  based on the element-wise formulas

$$\mathbf{J}_{\zeta_m^*}(i, j) = \prod_{d=1}^D \mathbf{c}'_{d,i} \mathbf{J}_{\phi_d} \mathbf{c}_{d,j} \quad (23)$$

$$\mathbf{R}_{\zeta_m^*}(i, j) = \sum_{d=1}^D \left( \prod_{b \neq d} \mathbf{c}'_{b,i} \mathbf{J}_{\phi_b} \mathbf{c}_{b,j} \right) \mathbf{c}'_{d,i} \mathbf{R}_{\phi_d} \mathbf{c}_{d,j} + \sum_{\substack{a,d \\ a \neq d}}^D \left( \prod_{\substack{b \neq a \\ b \neq d}} \mathbf{c}'_{b,i} \mathbf{J}_{\phi_b} \mathbf{c}_{b,j} \right) (\mathbf{c}'_{d,i} \mathbf{E}_{\phi_d} \mathbf{c}_{d,j}) (\mathbf{c}'_{a,i} \mathbf{E}_{\phi_a} \mathbf{c}_{a,j}). \quad (24)$$

Notably, due to the marginal product structure of  $\zeta_m^*$ , the  $D$ -dimensional integrals and partial derivatives required for the computation of  $\mathbf{J}_{\zeta_m^*}$  and  $\mathbf{R}_{\zeta_m^*}$  decompose into simple sums and products of integrals and partial derivatives over the marginal spaces. In contrast, computing such quantities for an arbitrary  $D$ -dimensional function is computationally prohibitive for moderately large  $D$ . This highlights an important practical advantage of working with the marginal product structure: it facilitates efficient computation of  $D$ -dimensional integrals and partial derivatives which can serve as primitives for developing fast two-stage algorithms for more complex FDA procedures.

In practice, we form estimates  $\widehat{\mathbf{C}}_d$  using MARGARITA and then estimate the inner product matrices  $\widehat{\mathbf{J}}_{\zeta_m^*}$  and  $\widehat{\mathbf{R}}_{\zeta_m^*}$  by plugging  $\widehat{\mathbf{C}}_d$  into (23) and (24), respectively. Standard FDA techniques for rank and penalty parameter selection can be adopted to select  $K^\ddagger$  and  $\lambda$ .

## 5 Simulation Study

### 5.1 Representing Random Marginal Product Functions

In this section, we compare three methods for constructing the functional representation of a random sample generated from a marginal product functional model: 1) a TPB system estimated by the sandwich smoother (Xiao et al., 2013), 2) the FCP-TPA algorithm (Allen, 2013), and 3) the  $K$ -oMPB estimated using MARGARITA. The two competitors are widely used for multidimensional function representation, see Section S4 of the Supplementary Text for more details.

The random function in our simulation is defined by the marginal product form:  $U(\mathbf{x}) = \sum_{k=1}^{K^t} A_k^t \prod_{d=1}^D (\mathbf{c}_{d,k}^t)' \phi_j^t(x_d)$ . Here  $\phi_j^t$  is the period-1 Fourier basis,  $\mathbf{c}_{d,k}^t$  is the  $k$ th column vector of  $\mathbf{C}_d^t$ , the fixed marginal factor matrix such that each element is an *i.i.d.* sample from  $\mathcal{N}(0, 0.3^2)$ ; and  $(A_1^t, \dots, A_{K^t}^t)' \sim \mathcal{N}(\mathbf{0}, \Sigma_A^t)$ . The covariance matrix is constructed as  $\Sigma_A^t = \mathbf{O}\mathbf{D}\mathbf{O}'$ , where  $\mathbf{O}$  is a random  $K^t \times K^t$  orthogonal matrix, and  $\mathbf{D}$  is a diagonal matrix with  $D_{kk} = \exp(-0.7k)$  for  $k = 1, \dots, K^t$ . We took the function domain to be the unit cube  $\mathcal{M} = [0, 1]^3$ . We fixed the true marginal basis dimensions to be  $m_d^t = 11$  for all  $d$  and considered true ranks  $K_t = 10$  and 20.

For both ranks, all combinations of the following sampling settings are considered. High vs low SNR; obtained by taking of  $\sigma^2$  to be 0.5 or 10, small vs. large domain sample size;  $n_d = 30$  or 50 for all  $d$ , respectively, and small vs. large subject sample size; where  $N$  is taken to be 5 or 50, respectively. For each of these settings, 100 replications are simulated according to Model (7). The performance of the fitting methods are assessed by computing the mean integrated squared error (MISE) for each replication  $r$ :  $\text{MISE}^{(r)} = \sum_{i=1}^{N^{(r)}} \int_{[0,1]^3} [U_i^{(r)}(\mathbf{x}) - \widehat{U}_i^{(r)}(\mathbf{x})]^2 d\mathbf{x}$ , where  $\widehat{U}_i^{(r)}$  is an estimate of  $U_i^{(r)}$  from the  $r$ th simulated dataset. Denote the Monte Carlo average of the MISE as  $\text{moMISE} = 100^{-1} \sum_{r=1}^{100} \text{MISE}^{(r)}$ .

For fitting, the second order derivative was used to define the marginal roughness penalties and a ridge penalty was used for regularization on the coefficients. Cubic b-splines were used as the marginal basis system.

We begin by investigating the performance as a function of rank for each combination of  $m_d \in \{15, 25\}$  and  $K_{\text{fit}} \in \{8, 15, 25\}$ . A fair comparison between the TPB and **MARGARITA** should be based on enforcing (roughly) equivalently sized parameter spaces, i.e. total number of degrees of freedom, so for TPB we take the smallest integer  $m_d^{(TPB)}$  such that  $\prod_{d=1}^D m_d^{(TPB)} \geq K_{\text{fit}} \sum_{d=1}^D m_d$  for comparison. To isolate the effects of the ranks, for each simulated dataset the models are estimated over a grid of smoothing parameters and the performance of the model with the lowest MISE is recorded. Section S5 in the Supplementary Text presents a comprehensive comparison of the moMISE for each simulation setting and model parameterization. The results demonstrate that **MARGARITA** outperforms its competitors consistently, particularly in comparison to TPB fits that have similar degrees of freedom.

Figure 1 presents a comparison of FCP-TPA and **MARGARITA** for each combination of  $m_d$  and  $K_{\text{fit}}$ , for several combinations of  $N$  and  $n_d$ , with  $K_t = 20$  and  $\sigma^2 = 10$ . While we see that in all cases **MARGARITA** results in fits with lower moMISE than FCP-TPA, we also observe that the ranks of the model have a significant impact on the performance. In practical settings, it is often necessary to automate the selection of these ranks as well as the smoothing parameters. Therefore, we compared the automated hyperparameter selection strategies for **MARGARITA** to the competitors automated smoothing approaches. Specifically, for the TPB method, we selected the smoothing parameters by minimizing the GCV criterion from Xiao et al. (2013). For FCP-TPA, we implemented a  $D$ -dimensional extension of the nested cross validation method from Huang et al. (2009), as suggested by the authors in Allen (2013). For our method, we selected penalty parameters using the cross validation scheme outlined in Algorithm 2 of the Supplemental Text. To focus our analysis, we consider the large domain large sample case ( $n_d = 50, N = 50$ ), with true rank  $K_t = 20$  for both low and high SNRs ( $\sigma^2 = 10, \sigma^2 = 0.5$ ) for 100 replications.

We use an elbow criteria to select the marginal ranks and set a threshold of  $\text{PVG}(K) \geq$



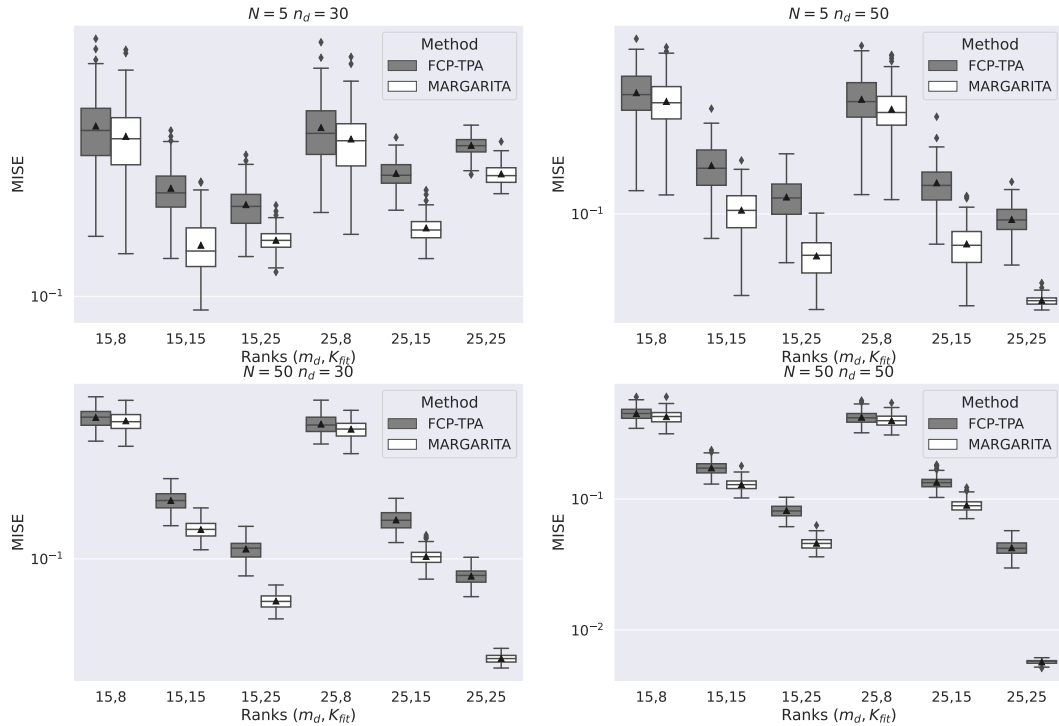


**Figure 1:** MISE of the fits resulting from both FCP-TPA (gray) and MARGARITA (white). moMISE is denoted by a triangle. The Y-axis is plotted on log-scale for clarity.

Method	FCP-TPA	MARGARITA	TPB
High SNR	$0.0729 \pm 0.0009$	$0.0418 \pm 0.0004$	$0.5927 \pm 0.0060$
Low SNR	$0.0886 \pm 0.0009$	$0.0458 \pm 0.0004$	$0.6681 \pm 0.0061$

**Table 1:** Monte Carlo average MISE for the  $n_d = 50, N = 50, K_t = 20$  regime for both high and low SNRs. Each methods proposed automatic penalty parameter selection method was used for estimation.

99.5% for global rank selection. The Monte-Carlo averages and standard error of these quantities are plotted for a range of  $m$  and  $K$  in the top right panels of Figures S1 and S2, respectively, found in the Supplemental Materials. We consistently identify a clear elbow at  $PVM(m) = 15$  for both SNRs, which is in line with the results in Figure 1 showing a significant increase in performance for  $m_d = 15$  compared to  $m_d = 8$ , while the performance boost from  $m_d = 15$  to  $m_d = 25$  is less pronounced. A  $K_{fit} = 25$  is consistently selected

across simulations. These ranks are fixed for subsequent comparison of the performance of smoothing parameter selection. Table 1 records the moMISE and accompanying standard errors for all methods, showing that MARGARITA’s automatic hyperparameter augmentation outperforms the competitors and is robust to noise. Furthermore, comparing these results to the corresponding results in the bottom right panel of Figure 1, we observe that our automated hyperparameter selection estimates models with similar performance to the ones obtained by selecting the oracle best fits over the hyperparameter grid.

Due to the super high-dimensional settings encountered, computational efficiency is as important a consideration as estimation performance in multidimensional FDA. Figure S4 in the Supplemental Text compares the computational time of FCP-TPA and MARGARITA for different simulation settings. We find that while both algorithms are comparable in computational speed for small  $N$  and small  $n_d$ , MARGARITA outperforms FCP-TPA as  $N$  and  $n_d$  increase. This trend is expected, since increasing  $n_d$  does not increase the dimension of the optimization problem (10), while the factors estimated with FCP-TPA are of dimension  $n_d$ , and thus the computational performance of the method can be expected to degrade as  $n_d$  increases and ultimately become infeasible in the fine grid limit.

## 5.2 Generalization Performance

In this section, we consider the generalization performance of MARGARITA, that is, how efficiently the  $K$ -oMPB estimated from a training sample of size  $N_{train}$  represents new realizations from the same distribution. The results of Section 2 indicate that we can expect near optimal generalization performance, with an inefficiency due to a “separability cost” that vanishes for increasing  $K$ . We compare our a method to the marginal product FPCA procedure proposed in Chen et al. (2017), referred to here as MargFPCA, which provides a similar near optimality result. In brief, MargFPCA constructs the marginal basis functions by applying FPCA to smoothed estimates of the marginal covariance functions.

The development of MargFPCA focuses on the  $D = 2$  case, so in this study we let the functional domain be  $\mathcal{M} = [0, 1]^2$  and evaluate the generalization error of both MARGARITA and MargFPCA as a function of  $N_{train}$  and  $K_{fit}$ . We define random function  $U$  to be a non-

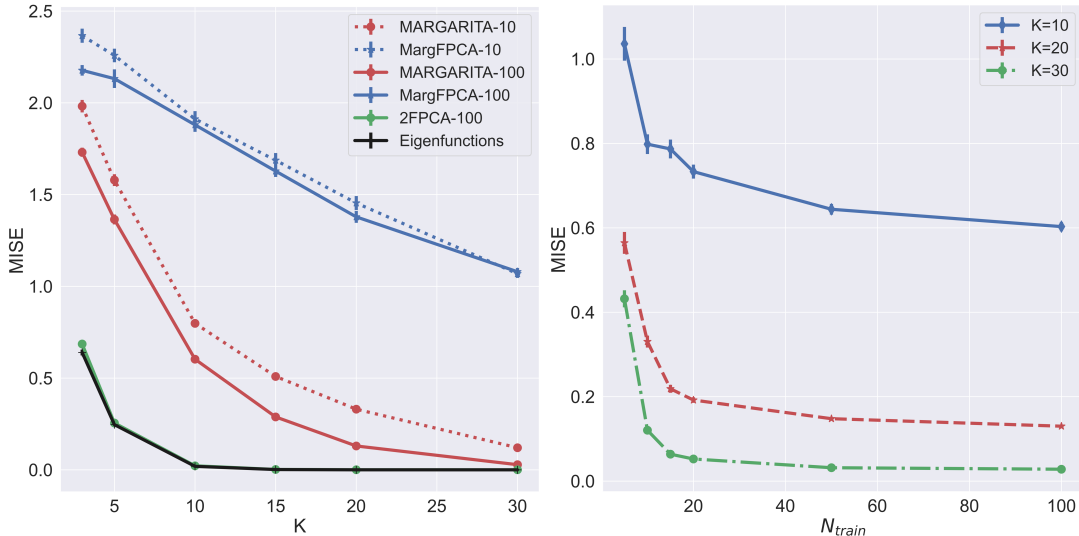


**Figure 2:** (left) Comparison of the generalization performance as a function of  $K$  for both MARGARITA (red) and MargFPCA (blue), for  $N_{train} = 10$  (dotted)  $N_{train} = 100$  (solid), as well as the 2-stage estimated (green) and true (black) eigenfunctions. (right) Generalization error of MARGARITA as a function  $N_{train}$  for several  $K$ .

stationary, non-separable anisotropic Gaussian process which is observed over an equispaced  $200 \times 200$  grid on  $\mathcal{M}$ . For each combination of  $N_{train}$  and rank  $K_{fit}$ , both MARGARITA and MargFPCA are used to construct the representations for each of 50 realizations from an independent test set using least squares basis expansion. Each experimental set-up is repeated for 25 replications. Additional details on the definition of  $U$  and other simulation settings can be found in Supplemental Section S5.2.

Figure 2 (left plot) displays the average MISE on the test set, i.e. the generalization error, as a function of  $K$  for both MARGARITA (red) and MargFPCA (blue). The dotted and solid lines correspond to  $N_{train} = 10$  and  $N_{train} = 100$ , respectively. For both training sample sizes, we observe that our method both uniformly outperforms MargFPCA for all ranks considered and displays much faster convergence in  $K$ . The green line shows the generalization performance of the eigenfunctions estimated using the two-stage FPCA procedure outlined in Section 4 for  $N_{train} = 100$ , with an initial MARGARITA of rank 60. The performance is nearly identical with that of the true eigenfunctions (black). Table S4 and Figure S5 in the Supplemental Material evaluate the two-stage estimates of first

three eigenfunctions, showing accurate recovery as  $N$  increases. The right plot of Figure 2 gives the average MISE as a function of  $N_{train}$  for several  $K$ . Recalling that MARGARITA is only guaranteed to converge to a local solution, these results indicate that, at least in some cases, the local (computable) solution still exhibits good convergence properties. Results for more ranks and training sample sizes are recorded in Section S5 of the Supplemental Materials and yield similar conclusions.

## 6 Real Data Analysis

The white matter (WM) of the human brain consists of large collections of myelinated neural fibers that permit fast communication between different regions of the brain. Diffusion magnetic resonance imaging (dMRI) is a non-invasive imaging technique which uses spatially localized measurements of the diffusion of water molecules to probe the WM microstructure. At each 3-dimensional voxel in the brain, the diffusion image can be used to compute scalar summaries of local diffusion, e.g. fractional anisotropy (FA) or mean diffusivity. The resulting data can be organized as a mode-3 tensor. For this application, we consider a dataset consisting of the brain images of 50 subjects in an age matched balanced case-control traumatic brain injury (TBI) study. Previous studies have shown the potential for using FA to identify white matter abnormalities associated with TBI and post concussive syndrome (Kraus et al., 2007). Typically, voxel-based analysis are performed for group-wise analysis of FA using Tract-Based Spatial Statistics (TBSS) (Smith et al., 2006), though such analysis are often not able to establish significant group differences (Khong et al., 2016), partially due to low power resulting from the large voxel-based multiple testing problem. Due to the continuity of the diffusion process, the FA tensor can be considered as discrete noisy observations of an underlying multidimensional random field, hence we may adopt the statistical model in Equation (7). In this analysis, we focus on a functional approach to predict disease status and identify regions in the WM which differ significantly between TBI and control. For details on the study design, MRI scanning protocol, and dMRI preprocessing, please visit Section S6 in the Supplementary Material.

The voxel grid is of size  $115 \times 140 \times 120$ . Point-wise estimates of the mean function

at each voxel are obtained using the sample mean tensor, which is then used to center the data. Equispaced cubic b-splines of ranks  $m_1 = 57, m_2 = 70, m_3 = 60$ , selected using a 90% threshold on the quantity described in Section 3.5, are used as marginal basis systems. Marginal roughness is penalized by the second order derivative and coefficients were regularized with a ridge penalty, with penalty parameters  $\lambda_d = 10^{-10}$  for  $d = 1, 2, 3$  and  $\lambda_4 = 10^{-8}$ . A rank  $K = 500$  model is estimated from the mean centered data tensor using MARGARITA. FPCA is then performed on the represented data using the fast two-stage approach outlined in Section 4. The first 45 eigenfunctions, denoted collectively as  $\psi$ , explain  $\approx 99\%$  of the represented variance and are used in constructing the final continuous representations of data. A lasso penalized logistic regression classifier is trained to predict disease status using the subject coefficient vectors obtained by their representation over  $\psi$ . The resulting classification performance is evaluated using leave-one-out cross validation (LOOCV). To localize group differences to particular eigenfunctions, univariate permutation test are performed on the coefficients and the resulting p-values are corrected to maintain a false discovery rate (FDR)  $\leq 5\%$  using Benjamini and Hochberg (1995). Finally, data-driven regions of interest (ROIs) are defined as spatial volumes where the values of the significant eigenfunctions are “extreme”, i.e. outside the 0.5% and 99.5% quantiles.

The LOOCV accuracy, precision and recall are 0.96, 1.0, and 0.92, respectively, indicating substantial discriminatory power of the learned basis functions. Additionally, the testing procedure identified significant group differences in the coefficients of three eigenfunctions. For comparison, we applied TBSS to this data and no significant group differences were identified. Figure 3 shows two cross sections of the brain, with the data-driven ROIs corresponding to the identified eigenfunctions displayed in blue, red and green. The ROIs in Figure 3 (a) are found within areas of the middle cerebellar peduncle (MCP) and, in Figure 3 (b), in areas along the superior longitudinal fasciculus (SLF) fiber bundle. Wang et al. (2016) found increased FA in the MCP is associated with increased cognitive impairment. Xiong et al. (2014) found decreased FA in the SLF in patients with TBI. We note that both of these studies were completed in acute cases of TBI, whereas our

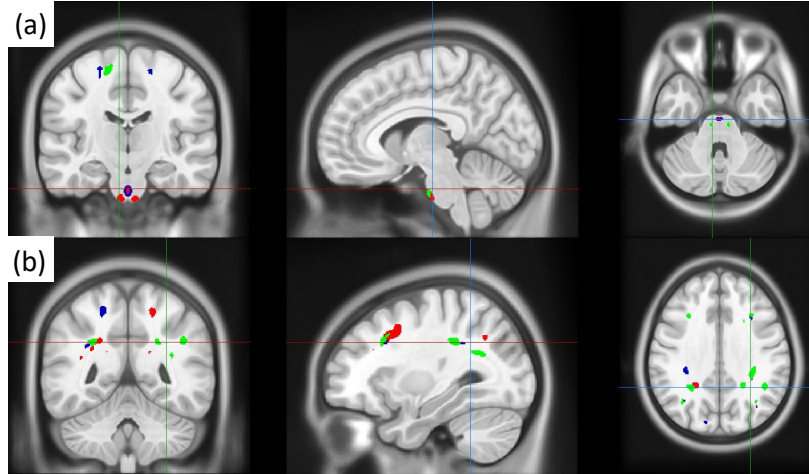


**Figure 3:** Data-driven ROIs created from thresholding the 0.5% and 99.5% quantiles of the three identified eigenfunctions in blue, red, and green.

data represents a more chronic state of TBI, often called post-concussive syndrome. That being said, these tracts are thought to be altered because of the nature of biophysical forces suffered in TBI. In all TBI, there is rotation of the head around the neck, which causes shearing and stretching of the brain stem tracts. In addition, the longer tracts in the brain, including the SLF, are subject to shearing forces on left to right rotation of the head around the neck. In fact, Post et al. (2013) found that mechanical strain in the brain stem and cerebellum are significantly correlated with angular acceleration of the brain, suggesting fibers in this area are susceptible to changes related to TBI. Therefore, our findings of changes in the MCP and SLF are consistent with the hypothesized mechanism and previous findings in TBI.

## 7 Discussion and Future Work

Our work introduces a methodological framework and accompanying estimation algorithm for constructing a flexible and efficient continuous representation of multidimensional functional data. We consider basis functions that exhibit a marginal product structure and prove that an optimal set of such functions can be defined by the penalized tensor decomposition of an appropriate transformation of the raw data tensor. A variety of separable roughness

penalties can be used to promote smoothness. Regularized parameter estimation is performed using a block coordinate descent scheme and we describe globally convergent numerical algorithms for solving the subproblems. Using extensive simulation studies, we illustrate the superiority of our proposed method compared to competing alternatives. In a real data application of the group-wise analysis of diffusion MRI, we show that our method can facilitate the prediction of disease status and identify biologically meaningful ROIs.

This work can be extended in several interesting directions. A principled and computationally efficient approach to both a generalized cross validation criteria and information criteria for faster penalty parameter selection and model-based selection of the global rank, respectively, are of interest. Additionally, many modern functional datasets are observed irregularly over the domain, rather than the common grid we consider here. To use our method on dense irregular data, we can bin the data using a common grid and define the observed data tensor to be the bin-specific sample means for each subject. However, this approach is problematic for sparsely sampled irregular data, requiring further extension of the method.

## References

- Allen, G. I. (2013). Multi-way functional principal components analysis. In *2013 5th IEEE International Workshop on Computational Advances in Multi-Sensor Adaptive Processing (CAMSAP)*, pp. 220–223.
- Allen, G. I. and M. Weylandt (2019). Sparse and functional principal components analysis. *2019 IEEE Data Science Workshop (DSW)*.
- Avants, B. B., N. Tustison, and G. Song (2009). Advanced normalization tools (ants). *Insight j* 2(365), 1–35.
- Bartels, R. H. and G. W. Stewart (1972). Solution of the matrix equation  $AX + XB = C$ . *Commun. ACM* 15(9), 820–826.
- Benjamini, Y. and Y. Hochberg (1995). Controlling the false discovery rate: A practical

- and powerful approach to multiple testing. *Journal of the Royal Statistical Society. Series B (Methodological)* 57(1), 289–300.
- Bertsekas, D. P. (1997). Nonlinear programming. *Journal of the Operational Research Society* 48(3), 334–334.
- Boyd, S., N. Parikh, E. Chu, B. Peleato, and J. Eckstein (2011, January). Distributed optimization and statistical learning via the alternating direction method of multipliers. *Found. Trends Mach. Learn.* 3(1), 1–122.
- Chen, K., P. Delicado, and H.-G. Müller (2017). Modelling function-valued stochastic processes, with applications to fertility dynamics. *Journal of the Royal Statistical Society: Series B (Statistical Methodology)* 79(1), 177–196.
- Chen, L.-H. and C.-R. Jiang (2017). Multi-dimensional functional principal component analysis. *Statistics and Computing* 27(5), 1181–1192.
- de Silva, V. and L.-H. Lim (2008). Tensor rank and the ill-posedness of the best low-rank approximation problem. *SIAM Journal on Matrix Analysis and Applications* 30(3), 1084–1127.
- Fonov, V., A. Evans, R. McKinstry, C. Almlí, and D. Collins (2009). Unbiased nonlinear average age-appropriate brain templates from birth to adulthood. *NeuroImage* 47, S102.
- French, J. (2020). *hero: Spatio-Temporal (Hero) Sandwich Smoother*. R package version 0.4.7.
- Happ, C. and S. Greven (2018). Multivariate functional principal component analysis for data observed on different (dimensional) domains. *Journal of the American Statistical Association* 113(522), 649–659.
- Hillar, C. J. and L.-H. Lim (2013). Most tensor problems are np-hard. *J. ACM* 60(6).
- Hsing, T. and R. Eubank (2015). *Theoretical foundations of functional data analysis, with an introduction to linear operators*. John Wiley & Sons.



- Huang, J. Z., H. Shen, and A. Buja (2009). The analysis of two-way functional data using two-way regularized singular value decompositions. *Journal of the American Statistical Association* 104(488), 1609–1620.
- Huang, K., N. D. Sidiropoulos, and A. P. Liavas (2016). A flexible and efficient algorithmic framework for constrained matrix and tensor factorization. *IEEE Transactions on Signal Processing* 64(19), 5052–5065.
- Khong, E., N. Odenwald, E. Hashim, and M. D. Cusimano (2016). Diffusion tensor imaging findings in post-concussion syndrome patients after mild traumatic brain injury: A systematic review. *Frontiers in Neurology* 7, 156.
- Kolda, T. G. and B. W. Bader (2009). Tensor decompositions and applications. *SIAM Review* 51(3), 455–500.
- Kraus, M. F., T. Susmaras, B. P. Caughlin, C. J. Walker, J. A. Sweeney, and D. M. Little (2007, 09). White matter integrity and cognition in chronic traumatic brain injury: a diffusion tensor imaging study. *Brain* 130(10), 2508–2519.
- Li, C., L. Xiao, and S. Luo (2020). Fast covariance estimation for multivariate sparse functional data. *Stat* 9(1), e245. e245 sta4.245.
- Li, Y., C. Huang, and W. K. Härdle (2019). Spatial functional principal component analysis with applications to brain image data. *Journal of Multivariate Analysis* 170, 263 – 274. Special Issue on Functional Data Analysis and Related Topics.
- Lynch, B. and K. Chen (2018). A test of weak separability for multi-way functional data, with application to brain connectivity studies. *Biometrika* 105(4), 815–831.
- Phan, A., P. Tichavský, and A. Cichocki (2013). Fast alternating ls algorithms for high order candecomp/parafac tensor factorizations. *IEEE Transactions on Signal Processing* 61(19), 4834–4846.
- Post, A., A. Oeur, B. Hoshizaki, and M. D. Gilchrist (2013). Examination of the relationship between peak linear and angular accelerations to brain deformation metrics in hockey

- helmet impacts. *Computer methods in biomechanics and biomedical engineering* 16(5), 511–519.
- Ramsay, J. O. and B. W. Silverman (2005). *Functional Data Analysis*. Springer-Verlag New York.
- Sidiropoulos, N. D. and R. Bro (2000). On the uniqueness of multilinear decomposition of n-way arrays. *Journal of Chemometrics* 14(3), 229–239.
- Silverman, B. W. (1996, 02). Smoothed functional principal components analysis by choice of norm. *The Annals of Statistics* 24(1), 1–24.
- Smith, S. M., M. Jenkinson, H. Johansen-Berg, D. Rueckert, T. E. Nichols, C. E. Mackay, K. E. Watkins, O. Ciccarelli, M. Z. Cader, P. M. Matthews, and T. E. Behrens (2006). Tract-based spatial statistics: Voxelwise analysis of multi-subject diffusion data. *NeuroImage* 31(4), 1487–1505.
- Stone, C. J. (1980). Optimal rates of convergence for nonparametric estimators. *The Annals of Statistics* 8(6), 1348–1360.
- Tibshirani, R. J. and J. Taylor (2012). Degrees of freedom in lasso problems. *The Annals of Statistics* 40(2), 1198 – 1232.
- Vaart, A. W. v. d. (1998). *Asymptotic Statistics*. Cambridge Series in Statistical and Probabilistic Mathematics. Cambridge University Press.
- Vaart, A. W. v. d. and J. A. Wellner (1996). *Weak Convergence and Empirical Processes: With Applications to Statistics*.
- Wang, J., R. K. W. Wong, and X. Zhang (2020). Low-rank covariance function estimation for multidimensional functional data. *Journal of the American Statistical Association* 0(0), 1–14.
- Wang, X. and C. Navasca (2015). Adaptive low rank approximation for tensors. In *2015 IEEE International Conference on Computer Vision Workshop (ICCVW)*, pp. 939–945.

- Wang, Z., W. Wu, Y. Liu, T. Wang, X. Chen, J. Zhang, G. Zhou, and R. Chen (2016). Altered cerebellar white matter integrity in patients with mild traumatic brain injury in the acute stage. *PLoS One* 11(3), e0151489.
- Wasserman, L. (2010). *All of Nonparametric Statistics*. Springer Publishing Company, Incorporated.
- Xiao, L., Y. Li, and D. Ruppert (2013). Fast bivariate p-splines: the sandwich smoother. *Journal of the Royal Statistical Society: Series B (Statistical Methodology)* 75(3), 577–599.
- Xiong, K., Y. Zhu, Y. Zhang, Z. Yin, J. Zhang, M. Qiu, and W. Zhang (2014). White matter integrity and cognition in mild traumatic brain injury following motor vehicle accident. *Brain research* 1591, 86–92.
- Zhang, J.-T. and J. Chen (2007). Statistical inferences for functional data. *The Annals of Statistics* 35(3), 1052 – 1079.

# SUPPLEMENTARY MATERIAL

## S1 Theory and Proofs

### Additional Definitions, Assumptions and Technical Conditions

**Definition S1.1.** Let the function  $w_{\phi_d}(m_d)$  be the  $\mathbb{L}^2(\mathcal{M}_d)$  convergence rate of the  $d$ th marginal basis system  $\phi_d$  and  $w_{\tau_m}(\mathbf{m})$  be the  $\mathbb{L}^2(\mathcal{M})$  convergence rate of the tensor product basis system  $\tau_m$ . That is, for any  $f_d \in \mathcal{H}_d$ ,  $f \in \mathcal{H}$

$$\left\| P_{\mathcal{H}_{m_d,d}^\perp}(f_d) \right\|_{\mathcal{H}_d} = O(w_{\phi_d}(m_d)), \quad \left\| P_{\mathcal{H}_m^\perp}(f) \right\|_{\mathcal{H}} = O(w_{\tau_m}(\mathbf{m}))$$

where  $P_{\mathcal{H}_{m_d,d}^\perp}$ ,  $P_{\mathcal{H}_m^\perp}$  are the projection operators onto  $\mathcal{H}_{m_d,d}^\perp$  and  $\mathcal{H}_m^\perp$ , the orthogonal complements of  $\mathcal{H}_{m_d,d}$  in  $\mathcal{H}_d$  and  $\mathcal{H}_m$  in  $\mathcal{H}$ , respectively.

**Definition S1.2.** For ease of presentation, we define the inner product space  $(\otimes_{d=1}^D \mathbb{R}^{m_d}, \langle \cdot, \cdot \rangle_{\bar{F}})$ , where  $\langle \mathcal{T}_1, \mathcal{T}_2 \rangle_{\bar{F}} = \langle \mathcal{T}_1, \mathcal{T}_2 \times_1 \mathbf{J}_{\phi_1} \cdots \times_D \mathbf{J}_{\phi_D} \rangle_F$  for  $\mathcal{T}_1, \mathcal{T}_2 \in \otimes_{d=1}^D \mathbb{R}^{m_d}$

We assume the following conditions related to the boundedness and tail-behavior of  $U$ .

*Assumption S2.*

$$(i) \quad \sum_{k=K+1}^{\infty} \sqrt{\rho_k} = o(1) \quad (ii) \quad \sum_{k=1}^{\infty} \mathbb{E} [|Z_k|^r] < \infty, \text{ for } r = 3, 4$$

Assumption S2.i introduces a slightly stronger condition on the decay rate of the eigenvalues than the one that comes for free from Assumption 1, i.e.  $\sum_{k=K+1}^{\infty} \rho_k = o(1)$ . Assumption S2.ii is a technical moment condition which controls the fatness of the ‘‘high-frequency tail’’ of  $U$ . These conditions are satisfied for many standard distributions and covariance kernels.

To ensure the existence and uniqueness of  $\check{\zeta}_{\mathbf{m},N}^*$ , we address the identifiability issues resulting from the inherent ambiguity in the ordering (permutation indeterminacy) of the basis functions. Since  $\zeta \in \mathcal{V}_{K,\mathbf{m}}$ , we have the representation  $\xi_{k,d}(x_d) = \sum_{j=1}^{m_d} c_{d,k,j} \phi_{d,j}(x_d)$ , and hence we can identify any  $\zeta \in \mathcal{V}_{K,\mathbf{m}}$  with the parameter  $(\mathbf{C}_1, \dots, \mathbf{C}_D)$ , where  $\mathbf{C}_d \in$

$\mathbb{R}^{m_d \times K}$  and  $\mathbf{c}_{d,k}$  is the  $k$ 'th column vector. We can now introduce the reparameterized relaxation of the parameter space  $\mathcal{V}_{K,m}$ :

$$\Theta_{K,m} := \{(\mathbf{C}_1, \dots, \mathbf{C}_D) : \mathbf{c}'_{d,k} \mathbf{J}_{\phi_d} \mathbf{c}_{d,k} \leq 1 \text{ for } d = 1, \dots, D; k = 1, \dots, K; \mathbf{C}_1(1,1) > \dots > \mathbf{C}_D(1,K)\}$$

which alleviates this identifiability problem. We must also address the ill-posedness of the best constrained rank approximations for  $D > 2$  in general (de Silva and Lim, 2008). We invoke a sufficient but not necessary condition on  $K$  to resolve this issue (Sidiropoulos and Bro, 2000):

*Assumption S3.* Let  $\mathcal{A}^{(K)}$  be the mode  $D+1$  tensor obtained from stacking  $\mathcal{A}_1, \dots, \mathcal{A}_K$  for some finite integer  $K$ . Suppose it's rank is  $K^*$ . We assume that  $K \geq (2K^* + D) / (D + 1)$ .

### Consistency

We establish the point-wise consistency of  $\check{\zeta}_{m,N}^*$ . Throughout this section, let  $0 < R < \infty$  be a generic constant, that is perhaps different depending on context. For notational convenience, we establish the following definition.

**Definition S1.3.** Let the function  $h(K)$  be convergence rate of the tail-sum of the eigenvalues of the covariance operator associated with  $C(\mathbf{x}, \mathbf{y})$ , that is

$$\sum_{k=K+1}^{\infty} \rho_k = O(h(K))$$

**Proposition S1.** *The coefficients of the projection  $P_{\zeta_m}(U) := \sum_{k=1}^K b_k \xi_k$  are given by*

$$\mathbf{b}_K := (b_1, \dots, b_K)' = \sum_{l=1}^{\infty} Z_l \mathbf{b}_l$$

where

$$\mathbf{b}_l = \begin{pmatrix} \prod_{d=1}^D \mathbf{c}'_{d,1} \mathbf{J}_{\phi_d} \mathbf{c}_{d,1} & \prod_{d=1}^D \mathbf{c}'_{d,1} \mathbf{J}_{\phi_d} \mathbf{c}_{d,2} & \cdots & \prod_{d=1}^D \mathbf{c}'_{d,1} \mathbf{J}_{\phi_d} \mathbf{c}_{d,K} \\ \prod_{d=1}^D \mathbf{c}'_{d,2} \mathbf{J}_{\phi_d} \mathbf{c}_{d,1} & \prod_{d=1}^D \mathbf{c}'_{d,2} \mathbf{J}_{\phi_d} \mathbf{c}_{d,2} & \cdots & \\ \vdots & & \ddots & \\ \prod_{d=1}^D \mathbf{c}'_{d,K} \mathbf{J}_{\phi_d} \mathbf{c}_{d,1} & \cdots & & \prod_{d=1}^D \mathbf{c}'_{d,K} \mathbf{J}_{\phi_d} \mathbf{c}_{d,K} \end{pmatrix}^{-1} \begin{bmatrix} \langle \mathcal{A}_l, \otimes_{d=1}^D \mathbf{c}_{d,1} \rangle_{\tilde{F}} \\ \langle \mathcal{A}_l, \otimes_{d=1}^D \mathbf{c}_{d,2} \rangle_{\tilde{F}} \\ \vdots \\ \langle \mathcal{A}_l, \otimes_{d=1}^D \mathbf{c}_{d,K} \rangle_{\tilde{F}} \end{bmatrix} \quad (\text{S.1})$$

and  $^{-1}$  refers to the (generalized) inverse of the inner product matrix.

*Proof.* This follows from the definition of the  $\mathbb{L}^2$  projection operator.  $\square$

**Proposition S2.** *Under Assumption 1, we have that (i)  $\mathbb{E} [\langle U, P_{\zeta_m}(U) \rangle_{\mathcal{H}}] < R$  and (ii)  $\mathbb{E} [\|P_{\zeta_m}(U)\|_{\mathcal{H}}^2] < R$  for any  $\zeta_m \in \mathcal{V}_{K,m}$ .*

*Proof.* The results follow immediately by noting that  $\|U\|_{\mathcal{H}}^2 \geq \|P_{\zeta_m}(U)\|_{\mathcal{H}}^2$  and  $\mathbb{E} [\|U\|_{\mathcal{H}}^2] = \sum_{k=1}^{\infty} \rho_k < \infty$ .  $\square$

**Lemma S3.** *The expected generalization error of  $\zeta_m \in \mathcal{V}_{K,m}$  can be written as*

$$\mathbb{E} \|U - P_{\zeta_m}(U)\|_{\mathcal{H}}^2 = \min_{\mathbf{B}} \left\| \mathcal{A}^{(K)} - \sum_{k=1}^K \left[ \bigotimes_{d=1}^D \mathbf{c}_{d,k} \right] \otimes \mathbf{B}_{:,k} \right\|_{\tilde{F},C}^2 + O(w_{\tau_m}(\mathbf{m})) + O(h(K)) \quad (\text{S.2})$$

where  $\mathbf{B}_{:,k}$  is the  $k$ 'th column of  $\mathbf{B} \in \mathbb{R}^{K \times K}$ , for some  $\mathbf{c}_{d,k} \in \mathbb{R}^{m_d}$ .

*Proof.*

$$\begin{aligned} \mathbb{E} \|U - P_{\zeta_m}(U)\|_{\mathcal{H}}^2 &= \mathbb{E} \|P_{\mathcal{H}_m}(U) - P_{\zeta_m}(U) + P_{\mathcal{H}_m^\perp}(U)\|_{\mathcal{H}}^2 \\ &= \mathbb{E} \|P_{\mathcal{H}_m}(U) - P_{\zeta_m}(U)\|_{\mathcal{H}_m}^2 + \\ &\quad + \mathbb{E} \langle (P_{\mathcal{H}_m}(U) - P_{\zeta_m}(U)), P_{\mathcal{H}_m^\perp}(U) \rangle_{\mathcal{H}} \\ &\quad + \mathbb{E} \|P_{\mathcal{H}_m^\perp}(U)\|_{\mathcal{H}_m^\perp}^2 \\ &:= \text{Term}_1 + \text{Term}_2 + \text{Term}_3. \end{aligned}$$

Term<sub>3</sub> is independent of  $\zeta_m$  and represents the expected irreducible error due to the finite dimensional truncation of the marginal basis systems. We have

$$\begin{aligned} \text{Term}_3 &= \mathbb{E} \|P_{\mathcal{H}_m^\perp}(U)\|_{\mathcal{H}_m^\perp}^2 = \mathbb{E} \left\| \sum_{k=1}^{\infty} Z_k P_{\mathcal{H}_m^\perp}(\psi_k) \right\|_{\mathcal{H}_m^\perp}^2 \\ &= \sum_{k=1}^{\infty} \mathbb{E} [Z_k^2] \cdot \|P_{\mathcal{H}_m^\perp}(\psi_k)\|_{\mathcal{H}_m^\perp}^2 \\ &= O(w_{\tau_m}(\mathbf{m})), \end{aligned} \quad (\text{S.3})$$

where the second line follows from the  $Z_k$  being uncorrelated and the third line follows since  $\sum_{k=1}^{\infty} \mathbb{E} [Z_k^2] = \sum_{k=1}^{\infty} \rho_k < \infty$ . Since  $\text{span}(\zeta_m) \subset \mathcal{H}_m$ , it is easy to see that Term<sub>2</sub> = 0 and thus we need only to deal with Term<sub>1</sub>.

The mapping  $\iota : \mathcal{H}_m \mapsto \bigotimes_{d=1}^D \mathbb{R}^{m_d}$  defined by  $\iota(u)_{j_1, \dots, j_D} = a_{j_1, \dots, j_D}$  is an isometry between inner product spaces  $(\mathcal{H}_m, \langle \cdot, \cdot \rangle_{\mathcal{H}_m})$  and  $(\bigotimes_{d=1}^D \mathbb{R}^{m_d}, \langle \cdot, \cdot \rangle_{\tilde{F}})$ , where  $a_{j_1, \dots, j_D}$  is the

coefficient of  $u$  associated with basis element  $\prod_{d=1}^D \phi_{d,j_d}$ . Recall that any  $u \in \text{span}(\zeta_m)$  has the representation

$$u(\mathbf{x}) = \sum_{k=1}^K b_k \prod_{d=1}^D \sum_{j=1}^{m_d} c_{k,d,j} \phi_{d,j}(x_d)$$

and hence, under  $\iota$ , is identified with the tensor rank- $K$  tensor  $\sum_{k=1}^K b_k \otimes_{d=1}^D \mathbf{c}_{d,k}$ , where  $\mathbf{c}_{d,k}$  are the  $m_d$ -vectors of coefficients for the  $k$ th marginal function in the  $d$ th dimension. It follows that

$$\begin{aligned} \mathbb{E} \|P_{\mathcal{H}_m}(U) - P_{\zeta_m}(U)\|_{\mathcal{H}_m}^2 &= \mathbb{E} \left\| \sum_{l=1}^{\infty} Z_l \mathcal{A}_l - \sum_{k=1}^K b_k \otimes_{d=1}^D \mathbf{c}_{d,k} \right\|_{\tilde{F}}^2 \\ &= \mathbb{E} \left\| \sum_{l=1}^{\infty} Z_l \mathcal{A}_l - \sum_{k=1}^K \sum_{j=1}^{\infty} Z_l b_{j,k} \otimes_{d=1}^D \mathbf{c}_{d,k} \right\|_{\tilde{F}}^2 \\ &= \mathbb{E} \left\| \sum_{l=1}^{\infty} Z_l \mathcal{A}_l - \sum_{k=1}^K Z_l b_{l,k} \otimes_{d=1}^D \mathbf{c}_{d,k} \right\|_{\tilde{F}}^2 \\ &= \sum_{l=1}^{\infty} \mathbb{E} [Z_l^2] \left\| \mathcal{A}_l - \sum_{k=1}^K b_{l,k} \otimes_{d=1}^D \mathbf{c}_{d,k} \right\|_{\tilde{F}}^2 \\ &\quad + \sum_{j \neq r} \mathbb{E} [Z_j Z_r] \left\langle \mathcal{A}_j - \sum_{k=1}^K b_{j,k} \otimes_{d=1}^D \mathbf{c}_{d,k}, \mathcal{A}_r - \sum_{k=1}^K b_{r,k} \otimes_{d=1}^D \mathbf{c}_{d,k} \right\rangle_{\tilde{F}} \\ &= \sum_{l=1}^{\infty} \rho_l \left\| \mathcal{A}_l - \sum_{k=1}^K b_{l,k} \otimes_{d=1}^D \mathbf{c}_{d,k} \right\|_{\tilde{F}}^2 \\ &= \sum_{l=1}^K \rho_l \left\| \mathcal{A}_l - \sum_{k=1}^K b_{l,k} \otimes_{d=1}^D \mathbf{c}_{d,k} \right\|_{\tilde{F}}^2 + O(h(K)) \\ &= \min_{\mathbf{B}} \sum_{k=1}^K \rho_l \left\| \mathcal{A}_l - \sum_{k=1}^K \mathbf{B}_{l,k} \otimes_{d=1}^D \mathbf{c}_{d,k} \right\|_{\tilde{F}}^2 + O(h(K)) \\ &= \min_{\mathbf{B}} \left\| \mathcal{A}^{(K)} - \sum_{k=1}^K \left[ \otimes_{d=1}^D \mathbf{c}_{d,k} \right] \otimes \mathbf{B}_{:,k} \right\|_{\tilde{F}, \mathcal{C}}^2 + O(h(K)). \end{aligned}$$

□

**Lemma S4.** *Let*

$$L_N(\mathbf{C}) := N^{-1} \sum_i^N \|U_i - P_{\mathbf{C}}(U_i)\|_{\mathcal{H}}^2; \quad L(\mathbf{C}) := \mathbb{E} \|U - P_{\mathbf{C}}(U)\|_{\mathcal{H}}^2.$$

where  $P_{\mathbf{C}}$  is the reparameterization of the projection operator  $P_{\zeta_{\mathbf{m}}}$  for  $\zeta_{\mathbf{m}}$  defined by  $\mathbf{C} = (\mathbf{C}_1, \dots, \mathbf{C}_D) \in \Theta_{K,m}$ . Define  $\check{\mathbf{C}}_N, \mathbf{C}^* \in \Theta_{K,m}$  to be the minimizers of  $L_N(\mathbf{C})$  and  $L(\mathbf{C})$ , respectively. Then

$$\check{\mathbf{C}}_N \xrightarrow{P} \mathbf{C}^*$$

*Proof.* The strong law of large numbers ensures  $L_N(\mathbf{C}) \rightarrow L(\mathbf{C})$  for every  $\mathbf{C}$ , almost surely. By Theorem 5.7 of Vaart (1998), the desired convergence holds if the following conditions are met:

1. *Uniform Convergence:*

$$\sup_{\mathbf{C} \in \Theta_{K,m}} |L_N(\mathbf{C}) - L(\mathbf{C})| \xrightarrow{P} 0$$

2. *Uniqueness:* For any  $\epsilon > 0$

$$\sup_{\mathbf{C} : \text{dist}(\mathbf{C}, \mathbf{C}^*) \geq \epsilon} L(\mathbf{C}) > L(\mathbf{C}^*)$$

3. *Near Minimum:*

$$L_N(\check{\mathbf{C}}_N) \leq L_N(\mathbf{C}^*) + o_P(1)$$

**Condition 1:** This can be verified by using Glivenko-Cantelli theory. Denote  $l_{\mathbf{C}}(U) = \|U - P_{\mathbf{C}}(U)\|_{\mathcal{H}}^2$ , i.e.  $L(\mathbf{C}) = \mathbb{E}[l_{\mathbf{C}}(U)]$ . Denote the set of functions

$$\Gamma = \{l_{\mathbf{C}} : \mathbf{C} \in \Theta_{K,m}\}.$$

The uniform convergence requirement is equivalent to  $\Gamma$  being Glivenko-Cantelli. We can express each element of the function set as

$$l_{\mathbf{C}}(u) = \|u\|_{\mathcal{H}}^2 - 2\langle u, P_{\mathbf{C}}(u) \rangle_{\mathcal{H}} + \langle P_{\mathbf{C}}(u), P_{\mathbf{C}}(u) \rangle_{\mathcal{H}}$$

Here, we work with the equivalent formulation of

$$\begin{aligned} l_{\mathbf{C}}(u) &= \|u\|_{\mathcal{H}}^2 - 2\langle u, P_{\mathbf{C}}(u) \rangle_{\mathcal{H}} + \langle P_{\mathbf{C}}(u), P_{\mathbf{C}}(u) \rangle_{\mathcal{H}} \\ &= \sum_{l=1}^{\infty} Z_q^2 - 2 \sum_{k=1}^K b_k \left\langle \sum_{q=1}^{\infty} Z_q \mathcal{A}_q, \bigotimes_{d=1}^D \mathbf{c}_{d,k} \right\rangle_{\tilde{F}} + \sum_{k=1}^K \sum_{p=1}^K b_k b_p \left\langle \bigotimes_{d=1}^D \mathbf{c}_{d,k}, \bigotimes_{d=1}^D \mathbf{c}_{d,p} \right\rangle_{\tilde{F}} \end{aligned} \quad (\text{S.4})$$



Recalling the definition of  $\langle \cdot, \cdot \rangle_{\tilde{F}}$  and we have

$$\begin{aligned} \left\langle \sum_{q=1}^{\infty} Z_q \mathcal{A}_q, \bigotimes_{d=1}^D \mathbf{c}_{d,k} \right\rangle_{\tilde{F}} &= \sum_{i_1=1}^{m_1} \cdots \sum_{i_D=1}^{m_D} \sum_{j_1=1}^{m_1} \cdots \sum_{j_D=1}^{m_D} \left( \sum_{q=1}^{\infty} Z_q \mathcal{A}_q(i_1, \dots, i_D) \right) \prod_{d=1}^D \mathbf{J}_{\phi_d}(i_d, j_d) \prod_{d=1}^D \mathbf{c}_{d,k,j_d} \\ \left\langle \bigotimes_{d=1}^D \mathbf{c}_{d,k}, \bigotimes_{d=1}^D \mathbf{c}_{d,p} \right\rangle_{\tilde{F}} &= \sum_{i_1=1}^{m_1} \cdots \sum_{i_D=1}^{m_D} \sum_{j_1=1}^{m_1} \cdots \sum_{j_D=1}^{m_D} \prod_{d=1}^D \mathbf{J}_{\phi_d}(i_d, j_d) \prod_{d=1}^D \mathbf{c}_{d,k,i_d} \mathbf{c}_{d,p,j_d} \end{aligned}$$

which are polynomials of order  $D$  and  $2D$  in  $\mathbf{C}$ , respectively. From the definition given in proposition S1, we can see that each  $b_k$  is also a finite degree polynomial in  $\mathbf{C}$ . As a result,  $l_{\mathbf{C}}(u)$  is isomorphic to a polynomial with finitely many terms. From the boundedness of the sum of the second moments of the  $Z_k$ 's along with proposition S2, it follows that  $\mathbb{E}[l_{\mathbf{C}}] < \infty$ . Therefore, the  $\Gamma$  is VC-class, which follows from Lemma 2.6.15 of Vaart and Wellner (1996), and hence Glivenko-Cantelli.

**Condition 2:** This condition indicates  $\mathbf{C}^*$  is a well separated minimum of  $L$ . Using Lemma S.2, we have that

$$\begin{aligned} \min_{\zeta_{\mathbf{m}} \in \mathcal{V}_{K,\mathbf{m}}} \mathbb{E} \|U - P_{\zeta_{\mathbf{m}}}(U)\|_{\mathcal{H}}^2 &= \min_{\mathbf{C} \in \Theta_{K,\mathbf{m}}} \min_{\mathbf{B}} \left\| \mathcal{A}^{(K)} - \sum_{k=1}^K \left[ \bigotimes_{d=1}^D \mathbf{c}_{d,k} \right] \otimes \mathbf{B}_{:,k} \right\|_{\tilde{F},\mathbf{C}}^2 + \\ &O(w_{\tau_{\mathbf{m}}}(\mathbf{m})) + O(h(K)) \end{aligned}$$

and therefore the minimizer of  $L$  is given by the rank  $K$  decomposition of the tensor  $\mathcal{A}^{(K)}$  under the  $\|\cdot\|_{\tilde{F},\mathbf{C}}$  norm. Under Assumption S3, this minimizer is unique in  $\Theta_{K,\mathbf{m}}$ . Coupled with the compactness of  $\Theta_{K,\mathbf{m}}$  and continuity of  $L$ , the desired condition follows.

**Condition 3:** This follows trivially, as

$$L_N(\check{\mathbf{C}}_N) = \min_{\mathbf{C} \in \Theta_{K,\mathbf{m}}} N^{-1} \sum_i^N \|U_i - P_{\mathbf{C}}(U_i)\|_{\mathcal{H}}^2 \leq N^{-1} \sum_i^N \|U_i - P_{\mathbf{C}^*}(U_i)\|_{\mathcal{H}}^2 = L_N(\mathbf{C}^*)$$

□

**Theorem S5 (Consistency).** *Under Assumptions 1 and S3, we have the following (component-wise) convergence result:*

$$\check{\zeta}_{\mathbf{m},N}^*(\mathbf{x}) \xrightarrow{P} \zeta_{\mathbf{m}}^*(\mathbf{x}) \quad \forall \mathbf{x} \in \mathcal{M}.$$

*Proof.* Note that  $\zeta_{\mathbf{m}}(\mathbf{x})$  is a continuous functions of  $\mathbf{C} \in \Theta_{K,\mathbf{m}}$  for all  $\mathbf{x} \in \mathcal{M}$ . The desired result follows directly from the convergence established in Lemma S4 and the continuous mapping theorem. □

## Convergence Rate

**Lemma S6** (Lipschitz Map). *Under Assumptions 1, S2 and S3, there exists functional  $F(u)$  such that  $\mathbb{E}[F^2] < \infty$  and*

$$|l_{\mathbf{C}^{(1)}}(u) - l_{\mathbf{C}^{(2)}}(u)| \leq F(u) \text{dist}(\mathbf{C}^{(1)}, \mathbf{C}^{(2)})$$

for any  $\mathbf{C}^{(1)}, \mathbf{C}^{(2)} \in \Theta_{K,m}$ , where  $\text{dist}(\mathbf{C}_1, \mathbf{C}_2) = \|\text{vec}(\mathbf{C}_1) - \text{vec}(\mathbf{C}_2)\|_2$ .

*Proof.* Notice that

$$\begin{aligned} |l_{\mathbf{C}^{(1)}}(u) - l_{\mathbf{C}^{(2)}}(u)| &= | -2\langle u, P_{\mathbf{C}^{(1)}}(u) - P_{\mathbf{C}^{(2)}}(u) \rangle_{\mathcal{H}} + \|P_{\mathbf{C}^{(1)}}(u)\|_{\mathcal{H}}^2 - \|P_{\mathbf{C}^{(2)}}(u)\|_{\mathcal{H}}^2 | \\ &\leq 2|\langle u, P_{\mathbf{C}^{(1)}}(u) - P_{\mathbf{C}^{(2)}}(u) \rangle_{\mathcal{H}}| + \| (P_{\mathbf{C}^{(1)}}(u)\|_{\mathcal{H}} - \|P_{\mathbf{C}^{(2)}}(u)\|_{\mathcal{H}}) (P_{\mathbf{C}^{(1)}}(u)\|_{\mathcal{H}} + \|P_{\mathbf{C}^{(2)}}(u)\|_{\mathcal{H}}) | \\ &\leq 2\|u\|_{\mathcal{H}} \|P_{\mathbf{C}^{(1)}}(u) - P_{\mathbf{C}^{(2)}}(u)\|_{\mathcal{H}} + \|P_{\mathbf{C}^{(1)}}(u) - P_{\mathbf{C}^{(2)}}(u)\|_{\mathcal{H}} (\|P_{\mathbf{C}^{(1)}}(u)\|_{\mathcal{H}} + \|P_{\mathbf{C}^{(2)}}(u)\|_{\mathcal{H}}) \\ &\leq 4\|u\|_{\mathcal{H}} \|P_{\mathbf{C}^{(1)}}(u) - P_{\mathbf{C}^{(2)}}(u)\|_{\mathcal{H}}. \end{aligned}$$

Additionally, we have that

$$\begin{aligned} \|P_{\mathbf{C}_1}(u) - P_{\mathbf{C}_2}(u)\|_{\mathcal{H}} &= \left\| \sum_{l=1}^{\infty} Z_l \sum_{k=1}^K (b_{l,k}^{(1)} \bigotimes_{d=1}^D \mathbf{c}_{d,k}^{(1)} - b_{l,k}^{(2)} \bigotimes_{d=1}^D \mathbf{c}_{d,k}^{(2)}) \right\|_{\tilde{F}} \\ &\leq \sum_{l=1}^{\infty} |Z_l| \sum_{k=1}^K \left\| (b_{l,k}^{(1)} \bigotimes_{d=1}^D \mathbf{c}_{d,k}^{(1)} - b_{l,k}^{(2)} \bigotimes_{d=1}^D \mathbf{c}_{d,k}^{(2)}) \right\|_{\tilde{F}} \quad (\text{S.5}) \\ &\leq R \sum_{l=1}^{\infty} |Z_l| \sum_{k=1}^K \left\| \bigotimes_{d=1}^D \mathbf{c}_{d,k}^{(1)} - \bigotimes_{d=1}^D \mathbf{c}_{d,k}^{(2)} \right\|_{\tilde{F}}. \end{aligned}$$

Clearly, the mapping defined by  $\mathbf{C} \mapsto \sum_{k=1}^K \left\| \bigotimes_{d=1}^D \mathbf{c}_{d,k} \right\|_{\tilde{F}}$  has bounded partial derivatives on  $\Theta_{K,m}$  and therefore is Lipschitz and hence

$$\sum_{k=1}^K \left\| \bigotimes_{d=1}^D \mathbf{c}_{d,k}^{(1)} - \bigotimes_{d=1}^D \mathbf{c}_{d,k}^{(2)} \right\|_{\tilde{F}} \leq R \|\text{vec}(\mathbf{C}_1) - \text{vec}(\mathbf{C}_2)\|_2.$$

Define  $F(u) := R\|u\|_{\mathcal{H}} \sum_{l=1}^{\infty} |Z_l|$  for generic constant  $0 < R < \infty$ . We have that

$$\begin{aligned}
\mathbb{E} [F^2] &= R\mathbb{E} \left[ \left( \sum_{l=1}^{\infty} Z_l^2 \right) \left( \sum_{l=1}^{\infty} |Z_l| \right)^2 \right] \\
&= R\mathbb{E} \left[ \sum_{l=1}^{\infty} \sum_{j=1}^{\infty} \sum_{q=1}^{\infty} Z_l^2 |Z_j| |Z_q| \right] \\
&= R \sum_{l=1}^{\infty} \sum_{j=1}^{\infty} \sum_{q=1}^{\infty} \mathbb{E} [Z_l^2] \mathbb{E} [|Z_j|] \mathbb{E} [|Z_q|] \mathbb{I}\{l \neq j, l \neq q, q \neq j\} + \\
&\quad \mathbb{E} [Z_l^2] \mathbb{E} [Z_q^2] \mathbb{I}\{l \neq j, j = q\} + \\
&\quad \mathbb{E} [|Z_l|^3] \mathbb{E} [|Z_j|] \mathbb{I}\{l \neq j, l = q\} + \\
&\quad \mathbb{E} [|Z_l|^3] \mathbb{E} [|Z_q|] \mathbb{I}\{l = j, l \neq q\} + \\
&\quad \mathbb{E} [Z_l^4] \mathbb{I}\{l = j = q\}.
\end{aligned}$$

Therefore,  $\sum_{l=1}^{\infty} \mathbb{E} [|Z_l|^r] < \infty$  for  $r = 1, 2, 3, 4 \implies \mathbb{E} [F^2] < \infty$ . Since  $\mathbb{E} [|Z_l|] \leq \sqrt{\rho_l}$  by Jensen's inequality, Assumptions 1 and S2 ensure each of these series are convergent and the desired result follows.  $\square$

**Theorem S7** (Convergence Rate). *Under Assumptions 1, S2 and S3, we have*

$$vec(\check{\mathbf{C}}_N) - vec(\mathbf{C}^*) = O_p(N^{-1/2})$$

*Proof.* This follows directly from combining lemmas S6 and S4 along with corollary 5.53 of Vaart (1998).  $\square$

## Generalization Error

### Proof of Theorem 2.1

*Proof.* By the triangle inequality,

$$\mathbb{E} \left\| U - P_{\zeta_{m,N}^*}(U) \right\|_{\mathcal{H}}^2 \leq \mathbb{E} \left\| U - P_{\zeta_m^*}(U) \right\|_{\mathcal{H}}^2 + \mathbb{E} \left\| P_{\zeta_m^*}(U) - P_{\zeta_{m,N}^*}(U) \right\|_{\mathcal{H}}^2 \quad (\text{S.6})$$

Let  $\boldsymbol{\psi}_K = (\psi_1, \dots, \psi_K)'$  and denote  $P_{\boldsymbol{\psi}_K}$  the projection operator onto  $\text{span}(\boldsymbol{\psi}_K)$ . For the first term in the bound (S.6), we have that

$$\begin{aligned}
\mathbb{E} \left\| U - P_{\zeta_m^*}(U) \right\|_{\mathcal{H}}^2 &= \mathbb{E} \left\| U - P_{\zeta_m^*}(U) + P_{\boldsymbol{\psi}_K}(U) - P_{\boldsymbol{\psi}_K}(U) \right\|_{\mathcal{H}}^2 \\
&\leq \mathbb{E} \left\| U - P_{\boldsymbol{\psi}_K}(U) \right\|_{\mathcal{H}}^2 + \mathbb{E} \left\| P_{\boldsymbol{\psi}_K}(U) - P_{\zeta_m^*}(U) \right\|_{\mathcal{H}}^2
\end{aligned} \quad (\text{S.7})$$

Clearly,  $\mathbb{E} \|U - P_{\psi_K}(U)\|_{\mathcal{H}}^2 = \sum_{k=K+1}^{\infty} \rho_k$ . Considering now the second term in the sum on line two of (S.7), observe that

$$\begin{aligned} \mathbb{E} \|P_{\psi_K}(U) - P_{\zeta_m^*}(U)\|_{\mathcal{H}}^2 &= \mathbb{E} \|P_{\mathcal{H}_m}(P_{\psi_K}(U) - P_{\zeta_m^*}(U)) + P_{\mathcal{H}_m^\perp}(P_{\psi_K}(U) - P_{\zeta_m^*}(U))\|_{\mathcal{H}}^2 \\ &= \mathbb{E} \|P_{\mathcal{H}_m}(P_{\psi_K}(U) - P_{\zeta_m^*}(U))\|_{\mathcal{H}_m}^2 + \mathbb{E} \|P_{\mathcal{H}_m^\perp}(P_{\psi_K}(U))\|_{\mathcal{H}_m^\perp}^2 \\ &= \text{Term}_1 + \text{Term}_2 \end{aligned}$$

Clearly,  $\text{Term}_2 = O(w_{\tau_m}(\mathbf{m}))$ . In regard to  $\text{Term}_1$ , using the same logic as in the proof of Lemma S3, we have that

$$\begin{aligned} \text{Term}_1 &= \min_{\mathbf{B}} \sum_{k=1}^K \rho_l \left\| \mathcal{A}_l - \sum_{k=1}^K \mathbf{B}_{l,k} \bigotimes_{d=1}^D \mathbf{c}_{d,k}^* \right\|_{\tilde{\mathcal{F}}}^2 \\ &= \min_{\mathbf{C} \in \Theta_{K,m}} \min_{\mathbf{B}} \sum_{l=1}^K \rho_l \left\| \mathcal{A}_l - \sum_{k=1}^K \mathbf{B}_{l,k} \bigotimes_{d=1}^D \mathbf{c}_{d,k} \right\|_{\tilde{\mathcal{F}}}^2 \\ &= \min_{\mathbf{C} \in \Theta_{K,m}} \min_{\mathbf{B}} \left\| \mathcal{A}^{(K)} - \sum_{k=1}^K \mathbf{B}_{l,k} \bigotimes_{d=1}^D \mathbf{c}_{d,k} \right\|_{\tilde{\mathcal{F}}, \mathbf{C}}^2 \\ &= \left\| \mathcal{A}^{(K)} - \tilde{\mathcal{A}}_K^{(K)} \right\|_{\tilde{\mathcal{F}}, \mathbf{C}}^2 \end{aligned}$$

where the last equality follows from the definition of the canonical polyadic decomposition, and the  $O(h(K))$  term from Lemma S3 is avoided due to the finite truncation of  $\psi_K$ . For the second term in the bound (S.6), using the Lipschitz property of the projection operators along with the rate in established in Theorem S7, it is easy to see that

$$\mathbb{E} \left\| P_{\zeta_m^*}(U) - P_{\zeta_{m,N}^*}(U) \right\|_{\mathcal{H}} = O_p(N^{-1/2}) \quad (\text{S.8})$$

The desired result follows from plugging the derived forms of  $\mathbb{E} \|U - P_{\psi_K}(U)\|_{\mathcal{H}}^2$ ,  $\text{Term}_1$ ,  $\text{Term}_2$  and (S.8) into Equation S.6.  $\square$

### Proof of Theorem 3.1

*Proof.*

$$\begin{aligned}
& \sum_{i=1}^N \left\| \mathcal{Y}_i - \sum_{k=1}^K \mathbf{B}_{ik} \bigotimes_{d=1}^D \Phi_d \mathbf{c}_{d,k} \right\|_F^2 = \left\| \mathcal{Y} - \sum_{k=1}^K \bigotimes_{d=1}^D \Phi_d \mathbf{c}_{d,k} \otimes \mathbf{b}_k \right\|_F^2 \\
& = \left\| \mathcal{Y} - \left[ \sum_{k=1}^K \bigotimes_{d=1}^D \mathbf{D}_d \mathbf{V}'_d \mathbf{c}_{d,k} \otimes \mathbf{b}_k \right] \times_1 \mathbf{U}_1 \times_2 \mathbf{U}_2 \cdots \times_D \mathbf{U}_D \right\|_F^2 \\
& = \left\| \hat{\mathcal{G}} - \left[ \sum_{k=1}^K \bigotimes_{d=1}^D \mathbf{D}_d \mathbf{V}'_d \mathbf{c}_{d,k} \otimes \mathbf{b}_k \right] \right\|_F^2.
\end{aligned}$$

Here the first equality is from properties of the Frobenius norm, the second comes from properties of  $d$ -mode multiplication, and the third from invariance of the Frobenius norm to orthogonal transformation. Therefore, solving Equation (9) is equivalent to solving

$$\min_{\mathbf{B}, \mathbf{C}} \left\| \hat{\mathcal{G}} - \sum_{k=1}^K \bigotimes_{d=1}^D \mathbf{D}_d \mathbf{V}'_d \mathbf{C}_d \otimes \mathbf{b}_k \right\|_F^2. \quad (\text{S.9})$$

Using the mapping  $\tilde{\mathbf{C}}_d = \mathbf{D}_d \mathbf{V}'_d \mathbf{C}_d$ , Equation (S.9) can be reparameterized as

$$\min_{\mathbf{B}, \tilde{\mathbf{C}}} \left\| \hat{\mathcal{G}} - \sum_{k=1}^K \bigotimes_{d=1}^D \tilde{\mathbf{C}}_d \otimes \mathbf{b}_k \right\|_F^2, \quad (\text{S.10})$$

which is solved by the rank- $K$  CPD of  $\hat{\mathcal{G}}$ . Comparing Equations (S.9) and (S.10), we see that  $\hat{\mathbf{B}} = \mathbf{B}$  and  $\mathbf{D}_d \mathbf{V}'_d \hat{\mathbf{C}}_d = \tilde{\mathbf{C}}_d$ , or equivalently,  $\hat{\mathbf{C}}_d = \mathbf{V}_d \mathbf{D}_d^{-1} \tilde{\mathbf{C}}_d$ .  $\square$

### Proof of Proposition 3.2

*Proof.* Let  $\mathbf{T}_d := \mathbf{D}_d^{-1} \mathbf{V}'_d \mathbf{R}_d \mathbf{V}_d \mathbf{D}_d^{-1} \in S_+^M$ , with  $\mathbf{R}_d(i, j) = \int_{\mathcal{M}_d} L_d(\phi_{d,i}) L_d(\phi_{d,j})$ , then

$$\begin{aligned}
& \sum_{k=1}^K \int_{\mathcal{M}_d} \sum_{d=1}^D \lambda_d L_d^2(\xi_{k,d}) = \sum_{d=1}^D \lambda_d \sum_{k=1}^K \mathbf{c}'_{d,k} \mathbf{R}_d \mathbf{c}_{d,k} \\
& = \sum_{d=1}^D \lambda_d \sum_{k=1}^K \tilde{\mathbf{c}}'_{d,k} \mathbf{D}_d^{-1} \mathbf{V}'_d \mathbf{R}_d \mathbf{V}_d \mathbf{D}_d^{-1} \tilde{\mathbf{c}}_{d,k} = \sum_{d=1}^D \lambda_d \text{tr}(\tilde{\mathbf{C}}'_d \mathbf{T}_d \tilde{\mathbf{C}}_d),
\end{aligned}$$

$\square$

## S2 MARGARITA Algorithm

Algorithm 1 provides pseudocode for MARGARITA. A couple comments are in order.

- For the ADMM subproblem, we adopt the stopping criteria proposed in Boyd et al. (2011) based on the primal and dual residuals at the  $r^{th}$  iteration, which have the form

$$r_{primal}^{(r)} = \|\mathbf{B}^{(r)} - \mathbf{Z}^{(r)'}\|_F, \quad r_{dual}^{(r)} = \|\gamma \left( \mathbf{Z}^{(r)} - \mathbf{Z}^{(r-1)} \right)\|_F. \quad (\text{S.11})$$

- As discussed, we can only guarantee convergence to a local minimum, and thus in practice it may be desirable to run Algorithm 1 for multiple random initializations and keep the best solution, e.g. evaluated using the proportion of variance explained criteria discussed in Section 3.5. In simulation results not reported, we did not find much difference in performance for a single random initialization vs. multiple random initializations, though this may become more important as the dimension of the domain  $D$  increases.
- In theory, the same ADMM scheme can be used to solve the special case of  $l() = \|\cdot\|_F^2$ , but this is not necessary in practice as an analytic solution exists. That said, for very large  $N$ , it may be the desirable to avoid an analytic solution as well due to the requirement of a large matrix inverse, i.e. see discussion in Section S3.2. In such cases, a more scalable solver, e.g. stochastic gradient descent, may be plugged into solve the  $\mathbf{B}$  sub-problem.

## S3 Hyper-Parameter Selection

### S3.1 Rank Selection

Data-driven methods for both marginal and global rank selection are important in practice, as they directly determine the approximation power of the resulting marginal product basis system, see Theorem 2.1. In the following, we provide an elaboration of

---

**Algorithm 1** MARGARITA: MARGinal-product bASIS Representation wIth Tensor Analysis

---

```

1: Input  $\mathcal{Y}, \mathcal{X}, \{\phi_{m_1,1}, \dots, \phi_{m_D,D}\}, \{L_1, \dots, L_D\}, \{\lambda_1, \dots, \lambda_{D+1}\}, K$ 
2: Output  $\mathbf{C}_1, \dots, \mathbf{C}_D, \mathbf{B}$ 
3: for  $d = 1, \dots, D$  do
4:   Compute  $\mathbf{T}_d$  using Proposition 3.2 and  $\Phi_d = \mathbf{U}_d \mathbf{D}_d \mathbf{V}_d'$  using  $\phi_d$  and  $\mathcal{X}$ 
5:   Randomly initialize  $\tilde{\mathbf{C}}_d$ 
6: Compute  $\hat{\mathcal{G}} = \mathcal{Y} \times_1 \mathbf{U}'_1 \times_2 \dots \times_D \mathbf{U}'_D$ , randomly initialize  $\mathbf{B}$  and set  $\mathbf{A}^*$  as zero matrix
7: while change in  $\tilde{\mathbf{C}}_1, \dots, \tilde{\mathbf{C}}_D, \mathbf{B}$  is non-negligible do
8:   for  $d = 1, \dots, D$  do
9:     Update  $\tilde{\mathbf{C}}_d$  according to (12), by way of (14) and re-scale to unit norm
10:  while  $r_{\text{primal}} > \text{tol}_{\text{primal}}$  or  $r_{\text{dual}} > \text{tol}_{\text{dual}}$  do
11:    Update  $\mathbf{B}$  according to (16)
12:    Update  $\mathbf{Z}$  according to (19)
13:    Update  $\mathbf{A}^*$  according to (18)
14:    Update  $r_{\text{primal}}, r_{\text{dual}}$  according to (S.11)
15: for  $d = 1, \dots, D$  do
16:   Get coefficient matrices using transformation  $\mathbf{C}_d = \mathbf{V}_d \mathbf{D}_d^{-1} \tilde{\mathbf{C}}_d$ 

```

---

and justification for the criteria used for the data-driven rank selection and evaluate their performance on simulated data from Section 5.

### S3.1.1 Marginal Rank

Recall that the proposed marginal rank selection criteria is defined as:  $\text{PVM}(\mathbf{m}) := \|\mathcal{Y} \times_{d=1}^D \mathbf{U}'_d\|_F^2 / \|\mathcal{Y}\|_F^2$ . Denote tensor  $\mathcal{U}_i \in \mathbb{R}^{n_1 \times \dots \times n_D}$  with element-wise definition  $\mathcal{U}_i(i_1, \dots, i_D) = U_i(x_{1,i_1}, \dots, x_{D,i_D})$ . Then the observation model in Equation (7) can be written as

$$\mathcal{Y}_i = \mathcal{U}_i + \mathcal{E}_i,$$

where  $\mathcal{E}_i$  is a tensor of isotropic normal errors with variance  $\sigma^2$ . The regression of  $\mathcal{U}_i$  onto the tensor product basis  $\boldsymbol{\tau}_m$  can be defined as

$$\mathcal{A}_i = \underset{\mathcal{A} \in \mathbb{R}^{m_1 \times \dots \times m_D}}{\text{argmin}} \left\| \mathcal{U}_i - \mathcal{A} \times_{d=1}^D \Phi_d \right\|_F^2, \quad (\text{S.12})$$

where  $\mathcal{A}_i$  is the coefficient tensor of  $\boldsymbol{\tau}_m$ . Recalling the notation of the SVD of the basis evaluation matrix  $\Phi_d := \mathbf{U}_d \mathbf{D}_d \mathbf{V}_d'$ , using properties of invariance of the norm, the least

squares objective can be written as

$$\begin{aligned} \left\| \mathcal{U}_i - \mathcal{A} \times_{d=1}^D \Phi_d \right\|_F^2 &= \left\| \mathcal{U}_i \times_{d=1}^D \mathbf{U}'_d - \left( \mathcal{A} \times_{d=1}^D \Phi_d \right) \times_{d=1}^D \mathbf{U}'_d \right\|_F^2 = \left\| \mathcal{U}_i \times_{d=1}^D \mathbf{U}'_d - \left( \mathcal{A} \times_{d=1}^D \mathbf{D}_d \mathbf{V}'_d \right) \right\|_F^2 \\ &= \left\| \mathbf{u}_{i,(d)}^* - (\mathbf{D}_D \mathbf{V}'_D \otimes \cdots \otimes \mathbf{D}_{d+1} \mathbf{V}'_{d+1} \otimes \mathbf{D}_{d-1} \mathbf{V}'_{d-1} \otimes \cdots \otimes \mathbf{D}_1 \mathbf{V}'_1)' \otimes \mathbf{D}_d \mathbf{V}'_d \text{vec}(\mathcal{A}_{(d)}) \right\|_F^2 \end{aligned}$$

where  $\mathbf{u}_{i,(d)}^*$  is shorthand for the vectorization of the  $d$ -mode unfolding of tensor, i.e.  $\mathbf{u}_{i,(d)}^* := \text{vec}([\mathcal{U}_i \times_{j=1}^D \mathbf{U}'_j]_{(d)})$ . By the properties of the Kronecker product, the design matrix  $(\mathbf{D}_D \mathbf{V}'_D \otimes \cdots \otimes \mathbf{D}_{d+1} \mathbf{V}'_{d+1} \otimes \mathbf{D}_{d-1} \mathbf{V}'_{d-1} \otimes \cdots \otimes \mathbf{D}_1 \mathbf{V}'_1)' \otimes \mathbf{D}_d \mathbf{V}'_d \in \mathbb{R}^{\prod_{d=1}^D m_d \times \prod_{d=1}^D m_d}$  is invertible, and so we have the exact solution:

$$\text{vec}(\mathcal{A}_{i,(d)}) = ((\mathbf{D}_D \mathbf{V}'_D \otimes \cdots \otimes \mathbf{D}_{d+1} \mathbf{V}'_{d+1} \otimes \mathbf{D}_{d-1} \mathbf{V}'_{d-1} \otimes \cdots \otimes \mathbf{D}_1 \mathbf{V}'_1)' \otimes \mathbf{D}_d \mathbf{V}'_d)^{-1} \mathbf{u}_{i,(d)}^*,$$

from which it follows that

$$\left\| \left( \mathcal{U}_i - \mathcal{A}_i \times_{d=1}^D \Phi_d \right) \times_{d=1}^D \mathbf{U}'_d \right\|_F^2 = 0.$$

Defining the tensor  $\mathcal{U}_i^\perp := \mathcal{U}_i - \mathcal{A}_i \times_{d=1}^D \Phi_d$ , the model for the  $i$ 'th subject can be equivalently written as

$$\mathcal{Y}_i = \mathcal{A}_i \times_{d=1}^D \Phi_d + \mathcal{U}_i^\perp + \mathcal{E}_i.$$

Now, the numerator of PVM( $\mathbf{m}$ ) can be written as

$$\begin{aligned} \left\| \mathcal{Y} \times_{d=1}^D \mathbf{U}'_d \right\|_F^2 &= \sum_{i=1}^N \left\| \mathcal{Y}_i \left( \times_{d=1}^D \mathbf{U}_d \mathbf{U}'_d \right) \right\|_F^2 \\ &= \sum_{i=1}^N \left\| \left( \mathcal{A}_i \times_{d=1}^D \Phi_d + \mathcal{U}_i^\perp + \mathcal{E}_i \right) \times_{d=1}^D \mathbf{U}_d \mathbf{U}'_d \right\|_F^2 \\ &= \sum_{i=1}^N \left\| \mathcal{A}_i \times_{d=1}^D \Phi_d + \mathcal{E}_i \times_{d=1}^D \mathbf{U}_d \mathbf{U}'_d \right\|_F^2. \end{aligned}$$



Putting this altogether, since  $\mathcal{U}_i \perp \mathcal{E}_i$  and independent for all  $i$ , asymptotically, we have that

$$\begin{aligned}
\text{PVM}(\mathbf{m}) &= \frac{N^{-1} \|\mathcal{Y} \times_{d=1}^D \mathbf{U}'_d\|_F^2}{N^{-1} \|\mathcal{Y}\|_F^2} \\
&= \frac{N^{-1} \sum_{i=1}^N \left\| \mathcal{A}_i \times_{d=1}^D \Phi_d + \mathcal{E}_i \times_{d=1}^D \mathbf{U}_d \mathbf{U}'_d \right\|_F^2}{N^{-1} \sum_{i=1}^N \|\mathcal{U}_i + \mathcal{E}_i\|_F^2} \\
&\asymp \frac{N^{-1} \sum_{i=1}^N \left\| \mathcal{A}_i \times_{d=1}^D \Phi_d \right\|_F^2 + N^{-1} \sum_{i=1}^N \left\| \mathcal{E}_i \times_{d=1}^D \mathbf{U}_d \mathbf{U}'_d \right\|_F^2}{N^{-1} \sum_{i=1}^N \|\mathcal{U}_i\|_F^2 + N^{-1} \sum_{i=1}^N \|\mathcal{E}_i\|_F^2} \\
&\asymp \frac{N^{-1} \sum_{i=1}^N \left\| \mathcal{A}_i \times_{d=1}^D \Phi_d \right\|_F^2 + \sigma^2 \prod_{d=1}^D n_d}{N^{-1} \sum_{i=1}^N \|\mathcal{U}_i\|_F^2 + \sigma^2 \prod_{d=1}^D n_d}
\end{aligned} \tag{S.13}$$

where the final line is due to

$$N^{-1} \sum_{i=1}^N \|\mathcal{E}_i\|_F^2 = N^{-1} \sum_{i=1}^N \left\| \mathcal{E}_i \times_{d=1}^D \mathbf{U}_d \mathbf{U}'_d \right\|_F^2 \asymp \sigma^2 \prod_{d=1}^D n_d,$$

which results from the permutation invariance of the trace and the strong law of large numbers.

Now, assuming a sequence of equipartitioned grids  $\mathcal{X}$ ,  $[\prod_{d=1}^D n_d]^{-1} \|\mathcal{U}_i\|_F^2$  can be considered proportional to a Riemann sum approximation to the integral  $\|\mathcal{U}_i\|_{\mathcal{H}}^2$ . Hence, under a fine grid regime, using the strong law of large numbers, recalling the notation from Section 2, we have the approximations

$$\begin{aligned}
N^{-1} \sum_{i=1}^N [\prod_{d=1}^D n_d]^{-1} \left\| \mathcal{A}_i \times_{d=1}^D \Phi_d \right\|_F^2 &\approx \mathbb{E}[\|P_{\mathcal{H}_m}(U)\|_{\mathcal{H}}^2] \\
N^{-1} \sum_{i=1}^N [\prod_{d=1}^D n_d]^{-1} \|\mathcal{U}_i\|_F^2 &\approx \mathbb{E}[\|U\|_{\mathcal{H}}^2].
\end{aligned}$$

For ease of presentation, from here on we take  $m_1 = \dots = m_D = m$  and  $n_1 = \dots = n_D = n$ . Then in the fine grid limit, we have the approximation

$$\text{PVM}(m) \asymp \frac{\mathbb{E}[\|P_{\mathcal{H}_m}(U)\|_{\mathcal{H}}^2] + \sigma^2}{\mathbb{E}[\|U\|_{\mathcal{H}}^2] + \sigma^2},$$

which is a monotonically increasing function of  $m$ , with  $\text{PVM}(m) \rightarrow 1$ , and measures the degree of irreducible bias incurred by the finite truncation of the marginal ranks. By

analogy, on the discretely observed grid,  $\text{PVM}(m)$  is a monotonic function of  $m \leq n$ , with  $\text{PVM}(n) = 1$  which is an approximation to the proportion of irreducible bias from the finite truncation of ranks under the discrete projection (S.12).

In practice, in the absence of strong a-priori knowledge, we suggest dividing each marginal domain into  $m = 1, \dots, M$  equispaced candidate ranks for each  $d$  and compute the  $\text{PVM}(m)$  for each of the  $M$  candidate marginal ranks  $\mathbf{m} := (\text{floor}(\frac{m}{M}n_1), \dots, \text{floor}(\frac{m}{M}n_D))$ . Figure S1 shows  $\text{PVM}(m)$  as a function of  $m$  under several of the simulation set-ups considered in Section 5. Cubic b-splines were used as the marginal basis of the fits for all the experiments. In order to study the effects of noise in both set-ups, we added iid Gaussian noise to the simulated fields in Section 5.2 with  $\sigma^2 = 0.1$  and  $\sigma^2 = 1$  for both relatively high and low  $\text{SNR} := \frac{\sum_k \rho_k}{\sigma^2}$ . We make the following observations:

1. We see that in the high SNR regimes, a proportion of variance explained or elbow criteria will both work. Alternatively, in the low signal to noise ratio regimes, the proportion of variance explained will select a larger model than necessary. Though “flatter” than that of the high SNR, the elbow of  $\text{PVM}(m)$  can still be consistently identified (even visually) in the low SNR simulations and thus we suggest using an elbow-like criteria in practice, especially when degrees of freedom need to be conserved.
2. For the simulation setup from Section 5.1 (top two plots), the true marginal basis are the Fourier functions while the marginal basis in fitting are the cubic b-splines. For both SNR’s, we see that a marginal b-spline basis with rank  $m = 15$  is consistently indentified with an elbow in the PVM for both noise levels. This is echoed in Table S1, where we see that the performance jump from  $m_d = 8$  to  $m_d = 15$  is substantial, while the over-parameterized regime  $m_d = 25$  performs quite similarly to  $m_d = 15$ .
3. For the simulation setup from Section 5.2 (bottom two plots), the true marginal ranks  $m_1 \neq m_2$ , hence, in theory, one direction will be “smoother” than the other. We again see a clear elbow at  $\max(m_1, m_2)=10$ . We also notice an inflection point at  $\max(m_1, m_2)=8$ , which may be a useful way of identifying when differing ranks are

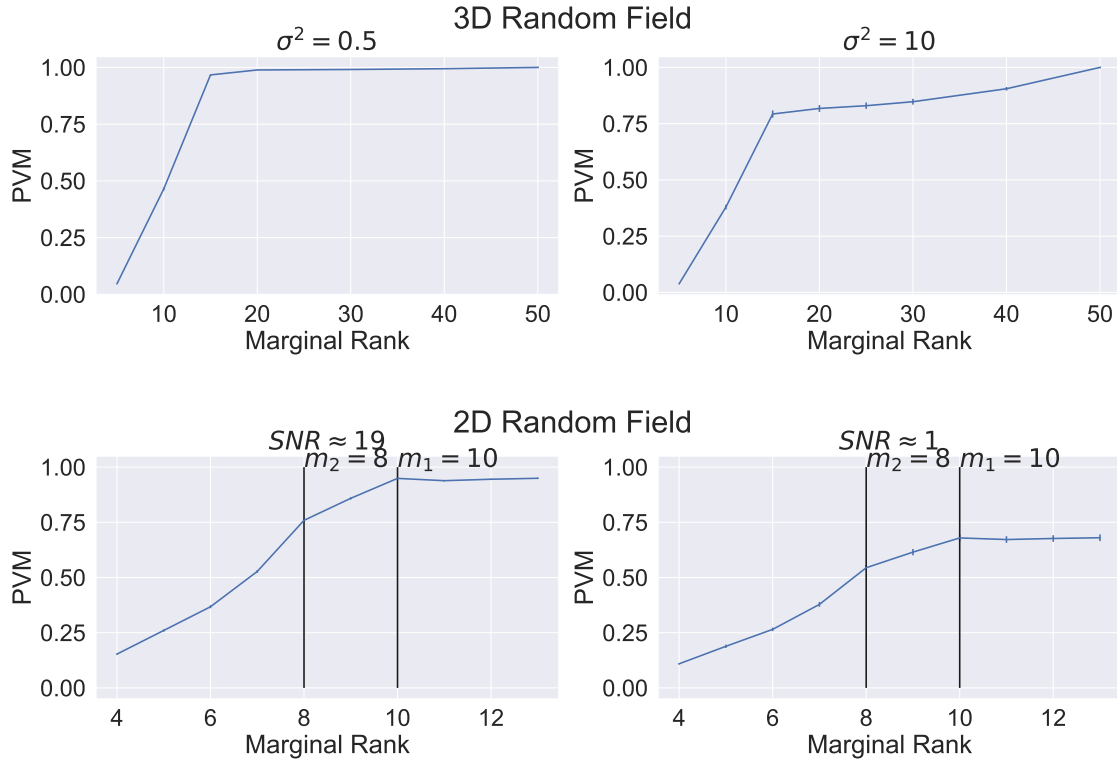


**Figure S1:** Monte-Carlo average PVM as a function of increasing  $m$ . The top two plots show the results from the 3D simulation set-up detailed in Section 5.1 with  $n_d = 50$ ,  $N = 50$  and  $K_t = 20$ . The bottom two plots show the results from the 2D simulation set-up from Section 5.2 with  $N = 100$ .

required in different directions, though the issue of which marginal domain requires which rank would need subsequent exploration.

We conclude this section by reiterating two significant advantages of the PVM criteria: i) it can be precomputed using only the SVD of a set of relatively small matrices ii) it is independent of the global rank  $K$ .

### S3.1.2 Global Rank

As discussed in the main text, a standard criteria for global rank selection is the proportion of variance explained, which in this context is given by

$$PVG(K) = \|\mathcal{G} - \sum_{k=1}^K \mathbf{b}_k \otimes (\bigotimes_{d=1}^D \tilde{\mathbf{c}}_{d,k})\|_F^2 / \|\mathcal{G}\|_F^2.$$

Computing the PVG requires multiple runs of **MARGARITA**, too many of which may want to be avoided in the super high-dimensional case. To avoid too many runs, one can start with some user-defined maximum rank  $K_{max}$  and then step backward in increments until the smallest model which still meets the desired PVG(K) is obtained. In simulations, we find that the PVG criteria is robust to changes in the SNR, see Figure S2. Computational resources permitting, we suggest the user to be generous with the PVG criteria, e.g. setting it very close to 1, to “soak up” most of the variance and then regularize via the cross-validation procedure discussed in Section S3.2. This is especially true if subsequent FPCA is desired and was the tactic for the two-stage estimation of the eigenfunctions in Section 5.2, which produces strong estimates for at least the first three eigenfunctions, see Figure S5. If desired, model selection in this case can be subsequently performed by selecting the rank on the second stage eigen-basis.

An interesting potential alternative path for global model selection is to encode the rank selection via a penalty operator and perform rank selection via selecting the penalty parameter  $\lambda_{D+1}$ . Specifically, we speculate that this may be accomplished by taking  $l(\mathbf{B}) = \sum_{k=1}^K \|\mathbf{B}(:, k)\|_2$ , the group lasso. Similar  $l_1$ -penalty based optimization strategies have been proposed for automatic approximate rank determination in the tensor decomposition literature (Wang and Navasca, 2015). **MARGARITA** can seamlessly integrate this penalty by simply specifying the corresponding proximal operator of the group lasso. That said, our approach to penalty parameter selection (discussed in Section S3.2) would need to be augmented for this purpose. As the rank of the model is not constant, for this case, it is desirable to adequately penalize a model complexity term in addition to a model fit term. As our method does not invoke a likelihood framework, there is no straightforward application of a standard information criteria for model selection, e.g. AIC or BIC.

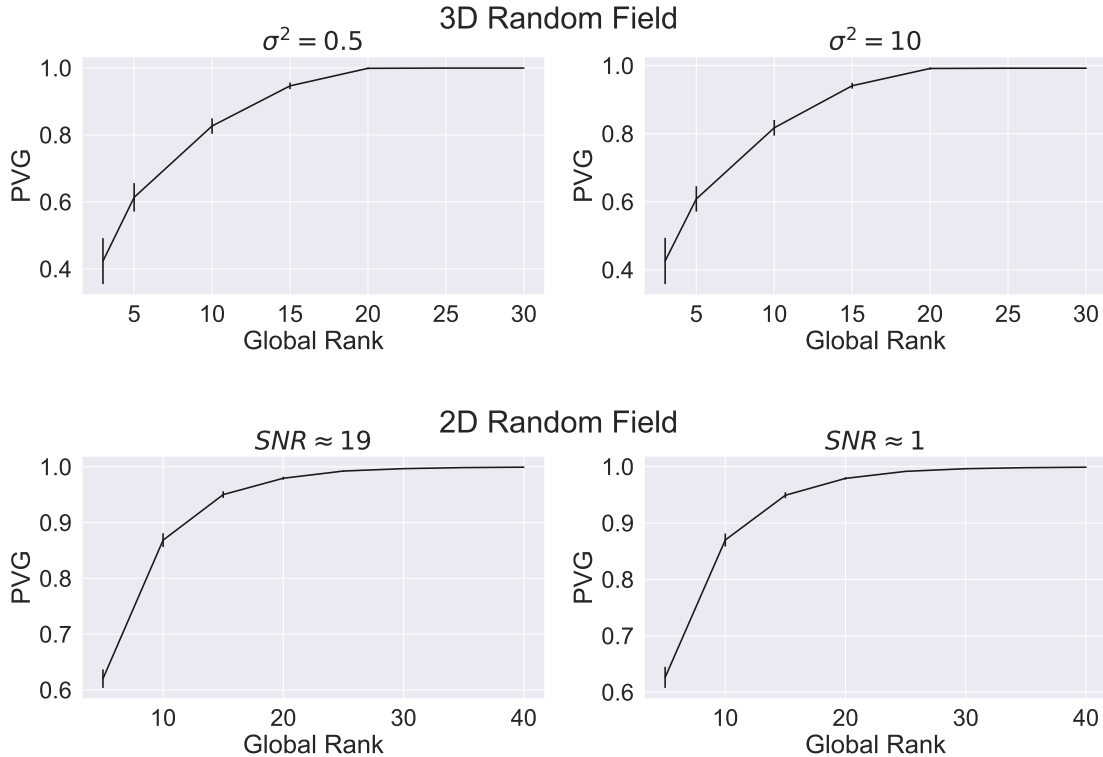


**Figure S2:** Monte-Carlo average PVG as a function of increasing  $K_{fit}$ . The top two plots show the results from the 3D simulation set-up detailed in Section 5.1 with  $n_d = 50, N = 50$  and  $K^t = 20$ . The bottom two plots show the results from the 2D simulation set-up from Section 5.2 with  $N = 100$ .

Therefore, developing a model selection criteria for our case is an important avenue for future research, but is beyond the scope of the current work.

### S3.2 Penalty Strength Selection via Cross Validation

Multidimensional functional data analysis is notoriously high-dimensional, and therefore the consideration of the statistical validity of a selection procedure must always be balanced with considerations of the computational efficiency. Although MARGARITA allows all  $D+1$  penalty parameters to be specified independently, in the absence of problem specific a-priori information, we suggest to let  $\lambda_d = \lambda_f$  for  $d = 1, \dots, D$  and then select  $(\lambda_f, \lambda_{D+1})'$  by minimizing the  $T$ -fold cross-validation error over a 2-dimensional grid of potential values.

---

**Algorithm 2 CV-MARGARITA**


---

- 1: **Input**  $\mathcal{Y}, \mathcal{X}, \{\phi_{m_1,1}, \dots, \phi_{m_D,D}\}, \{L_1, \dots, L_D\}$ , candidate set  $\{(\lambda_f, \lambda_{D+1})\}$ , global rank  $K$ , number of folds  $T$
- 2: **Output** Selected smoothing parameters  $(\lambda_f^*, \lambda_{D+1}^*)$
- 3: Partition the observed data tensor into  $T$ -folds  $\{\mathcal{Y}^{(1)}, \dots, \mathcal{Y}^{(T)}\}$ , where  $\mathcal{Y}^{(t)} \in \mathbb{R}^{n_1 \times \dots \times n_D \times N_t}$ . Denote  $\mathcal{Y}^{(-t)}$  the tensor with all but the  $\mathcal{Y}^{(t)}$  fold.
- 4: Compute  $\mathbf{T}_d$  using Proposition 3.2 and  $\Phi_d = \mathbf{U}_d \mathbf{D}_d \mathbf{V}_d'$  using  $\phi_d$  and  $\mathcal{X}$
- 5: **for** each candidate parameter  $(\lambda_f, \lambda_{D+1})$  **do**
- 6:     **for**  $t = 1, \dots, T$  **do**
- 7:         Apply Algorithm 1 with  $\mathcal{Y}^{(-t)}$  penalty parameters  $(\lambda_1 = \lambda_f, \dots, \lambda_D = \lambda_f, \lambda_{D+1})$  to obtain  $\mathbf{C}_1^{(-t)}, \dots, \mathbf{C}_D^{(-t)}, \mathbf{B}^{(-t)}$
- 8:         Form tensor  $\mathcal{Z}^{(-t)} \in \mathbb{R}^{n_1 \times \dots \times n_D \times K}$ , with element-wise definition

$$\mathcal{Z}_{k,i_1,\dots,i_D}^{(-t)} = \prod_{d=1}^D \xi_{k,d}^{(-t)}(x_{d,i_d}), \quad \xi_{k,d} = \sum_{j=1}^{m_d} \mathbf{C}_d^{(-t)}(k,j) \phi_{d,j}$$

- 9:         Compute the tensor regression on the held-out data:

$$\widehat{\mathbf{B}}^{(t)} := \min_{\mathbf{B}^{(t)}} \left\| \mathcal{Y}^{(t)} - \mathcal{Z}^{(-t)} \times_{D+1} \mathbf{B}^{(t)} \right\|_F^2 + \lambda_{D+1} l(\mathbf{B}^{(t)}), \quad (\text{S.15})$$

- 10:         Form the cross-validation error

$$\text{CV}^{(t)}(\lambda_f, \lambda_{D+1}) = \left\| \mathcal{Y}^{(t)} - \mathcal{Z}^{(-t)} \times_{D+1} \mathbf{B}^{(t)} \right\|_F^2,$$

- 11: Set  $(\lambda_f^*, \lambda_{D+1}^*)$  which minimizes  $\sum_{t=1}^T \text{CV}^{(t)}$
- 

To make things explicit, we provide pseudo-code for the automated smoothing parameter selection, referred to as CV-MARGARITA, in Algorithm 2. Notice that using the tensor unfolding operator (Kolda and Bader, 2009), the high-dimensional regression (S.15) can be re-written as

$$\begin{aligned} \widehat{\mathbf{B}}^{(t)} &:= \min_{\mathbf{B}^{(t)}} \left\| \mathbf{Y}_{(D+1)}^{(t)} - \mathbf{B}^{(t)} \mathbf{Z}_{(D+1)}^{(-t)} \right\|_F^2 + \lambda_{D+1} l(\mathbf{B}^{(t)}) \\ &= \min_{\mathbf{B}^{(t)}} \left\| \mathbf{Y}_{(D+1)}^{(t)'} - \mathbf{Z}_{(D+1)}^{(-t)'} \mathbf{B}^{(t)'} \right\|_F^2 + \lambda_{D+1} l(\mathbf{B}^{(t)}) \end{aligned} \quad (\text{S.14})$$

Now, (S.14) has the form of Equation (13) from the main text, and hence can be solved (globally) using the same ADMM scheme discussed in Section 3.4 for general  $l(\cdot)$ , or in closed form for the special case of  $l(\cdot) = \|\cdot\|_F^2$ .

We now provide some justification for our approach to smoothing parameter selection by considering some of the tactics used in related work. Several works (Huang et al., 2009; Allen, 2013; Allen and Weylandt, 2019) propose the integration of penalty selection into the coordinate-wise updates of the estimation algorithm, using the so-called nested generalized

cross validation. In the following, we derive an analogous procedure for coordinate-wise updating for all factor matrices and then discuss why we recommend our **CV-MARGARITA** instead.

We start with the  $\tilde{\mathbf{C}}_d$  parameters. Using properties of the  $\text{vec}$  operator and the permutation invariance of the trace, it is easy to show that the objective function for the optimization problem in Equation (12) can be vectorized into a high dimensional ridge-type regression as follows:

$$\begin{aligned}
& \|\text{vec}(\mathbf{G}_{(d)}) - \text{vec}(\mathbf{W}_d^{(r)} \tilde{\mathbf{C}}_d')\|_F^2 + \lambda_d \text{tr}(\tilde{\mathbf{C}}_d \mathbf{T}_d \tilde{\mathbf{C}}_d') \\
&= \|\text{vec}(\mathbf{G}_{(d)}) - (\mathbf{I}'_{m_d} \otimes \mathbf{W}_d^{(r)}) \text{vec}(\tilde{\mathbf{C}}_d')\|_F^2 + \lambda_d \text{tr}((\mathbf{T}_d^{1/2} \tilde{\mathbf{C}}_d')' \mathbf{T}_d \tilde{\mathbf{C}}_d') \\
&= \|\text{vec}(\mathbf{G}_{(d)}) - (\mathbf{I}'_{m_d} \otimes \mathbf{W}_d^{(r)}) \text{vec}(\tilde{\mathbf{C}}_d')\|_F^2 + \lambda_d \text{vec}(\tilde{\mathbf{C}}_d')' (\mathbf{I}_K \otimes \mathbf{T}_d) \text{vec}(\tilde{\mathbf{C}}_d').
\end{aligned} \tag{S.16}$$

The corresponding ‘‘hat’’ matrix is given by

$$\mathbf{H}_d(\lambda) = (\mathbf{I}'_{m_d} \otimes \mathbf{W}_d) [(\mathbf{I}'_{m_d} \otimes \mathbf{W}_d)' (\mathbf{I}'_{m_d} \otimes \mathbf{W}_d) + \lambda_d (\mathbf{I}_K \otimes \mathbf{T}_d)]^{-1} (\mathbf{I}'_{m_d} \otimes \mathbf{W}_d')$$

In order to compute a generalized cross validation selection criteria, we need to obtain a measure of the degrees of freedom of the model. In the ridge regression set-up, this requires the computation of the trace, given by

$$\text{tr}(\mathbf{H}_d(\lambda)) = \text{tr}((\mathbf{I}_{m_d} \otimes \mathbf{W}_d' \mathbf{W}_d) [(\mathbf{I}_{m_d} \otimes \mathbf{W}_d' \mathbf{W}_d) + \lambda_d (\mathbf{I}_K \otimes \mathbf{T}_d)]^{-1}). \tag{S.17}$$

For the  $\mathbf{B}$  parameters, under the special case of  $l(\cdot) = \|\cdot\|_2^2$ , we have a similar structure to (S.16), with  $\mathbf{T}_{D+1} := \mathbf{I}_N$ , and hence the previous analysis holds. For the case when  $l(\cdot) = \|\cdot\|_1$ , Equation (13) can be unfolded into a high-dimensional Lasso regression problem, and hence the degrees of freedom can be quantified using, e.g. the measure from Tibshirani and Taylor (2012).

All this said, integrating this nested procedure to solve the hyper-parameter selection problem is non-trivial. First, notice that computation of the trace requires the inversion of a  $m_d K \times m_d K$  matrix, for each candidate  $\lambda_d$ , at each iteration of **MARGARITA**. This may not be a problem for relatively small models, but is undesirable for large models. Note that the approaches in (Allen, 2013; Huang et al., 2009; Allen and Weylandt, 2019) are deflationary approaches which perform a series of rank-1 approximations, and thus do

not encounter this issue. Furthermore, care must be taken to avoid convergence issues, as the convergence of the sub-problems in MARGARITA, which is currently guaranteed as discussed in Section 3.4 of the main text, may no longer hold. This potential issue is noted in Allen and Weylandt (2019), though no rigorous proposal is made in order to guard against it. Integrating a nested procedure may be an interesting avenue for future work, but the potential convergence problems as well as the previously highlighted potential computational issues related to the matrix inversion for the large  $m_d, K$  case will need to be rigorously handled, which is well beyond the scope of the current work.

## S4 Brief Overview of Competing Methods

The so-called *sandwich smoother*, introduced by Xiao et al. (2013), is a method for estimating the coefficients of a tensor product approximation to an unknown deterministic function from noisy observations on a grid. The main contribution is in a clever formulation of the penalty term, which allows for the fast computation of the GCV statistic and hence a computationally efficient technique for selecting the roughness penalty strength. For more information, see the aforementioned paper or the `hero` package in R (French, 2020).

We give a brief overview of the FCP-TPA algorithm (Allen, 2013), which is essentially a  $D$ -dimensional extension of the 2-dimensional regularization scheme from Huang et al. (2009). Using our notation, the FCP-TPA estimates the  $k$ th *MPB basis evaluation vectors*  $\Xi_{d,k}$  and associated coefficient vector  $\mathbf{b}_k$  by solving a series of  $K$  rank-one penalized decompositions of the residual tensor. That is, at the  $k$ th iteration, FCP-TPA solves problem

$$\min_{\Xi_{1,k}, \dots, \Xi_{D,K}, \mathbf{b}_k} \left\| \mathcal{Y}_{resid} - \bigotimes_{d=1}^D \Xi_{d,k} \otimes \mathbf{b}_k \right\|_F^2 - \prod_{d=1}^D \left\| \Xi_{d,k} \right\|_2^2 + \prod_{d=1}^D \Xi_{d,k}' \mathbf{P}_d^{-1} \Xi_{d,k} \quad (\text{S.18})$$

where  $\mathcal{Y}_{resid} = \mathcal{Y} - \sum_{j=1}^{k-1} \bigotimes_{d=1}^D \Xi_{d,j} \otimes \mathbf{b}_j$  and  $\mathbf{P}_d \in \mathbb{R}^{n_d \times n_d}$  is a smoothing matrix, e.g. derived using squared second order differences. The solution to (S.18) is approximated using a series of rank-1 approximations, each of which are solved using tensor power iterations which are shown to converge to a stationary point.



Note that FCP-TPA does not directly construct a continuous representation but rather the discrete evaluations of the optimal marginal product functions on the observed marginal grid, i.e. the  $\Xi_d$ 's. In order to obtain a continuous representation from the output of FCP-TPA, a “decompose-then-represent” approach is used in which the marginal basis functions are estimated from the basis expansion of the  $\Xi_d$ 's.

## S5 Additional Simulation Studies and Details

All simulations were performed using R/4.0.2 and Python/3.8.16 on a Linux machine equipped with a 2.4 GHz Intel Xeon CPU E5-2695 and 24GB of RAM.

### S5.1 Additional Comparisons to TPB and FCP-TPA

Figure S3 and Table S1 display comparisons of the performance between MARGARITA and the tensor product basis (TPB) estimated by the sandwich smoother for all simulation settings considered. We note substantially better performance for MARGARITA over TPB for comparable degrees of freedom, given by  $\prod_{d=1}^D m_d$  and  $K_{\text{fit}} \sum_{d=1}^D m_d$  for the TPB and MARGARITA, respectively.

Table S2 displays the relative difference in moMISE, defined as

$$\frac{\text{moMISE}_{\text{FCP-TPA}} - \text{moMISE}_{\text{MARGARITA}}}{\text{moMISE}_{\text{FCP-TPA}}} \quad (\text{S.19})$$

between the fits resulting from the FCP-TPA algorithm and MARGARITA for all marginal and global ranks and simulation settings. As all but one of the entries in the table is positive, MARGARITA is nearly uniformly outperforming the FCP-TPA. We see that the relative boost in performance from MARGARITA generally increases with  $K_{\text{fit}}$  and marginal rank  $m_d$ .

Figure S4 displays a comparison of the computational time between FCP-TPA and MARGARITA for a variety of model and data sizes. We note that the methods exhibit comparable performance for the small sample, small domain case, while MARGARITA is much faster for the large sample, large domain case.

**Table S1:** moMISE comparison of MARGARITA (a), to the tensor product basis estimated by sandwich smoother (b).

(a) Marginal Product Basis

$K_{true}$	$\sigma^2$	$N$	$n_d$	$K_{fit} = 15$			$K_{fit} = 25$		
				$m_d$ (model d.o.f.)					
				8 (360)	15 (675)	25 (1,125)	8 (600)	15 (1,125)	25 (1,875)
10	0.5	5	30	0.0890	0.0433	0.0433	0.0511	0.0030	0.0033
10	0.5	5	50	0.0932	0.0405	0.0402	0.0560	0.0006	0.0006
10	0.5	50	30	0.1186	0.0426	0.0411	0.0790	0.0017	0.0007
10	0.5	50	50	0.1196	0.0398	0.0394	0.0757	0.0001	0.0001
10	10.0	5	30	0.1148	0.1049	0.1634	0.1039	0.0919	0.1579
10	10.0	5	50	0.0976	0.0530	0.0647	0.0616	0.0180	0.0312
10	10.0	50	30	0.1166	0.0525	0.0632	0.0800	0.0146	0.0263
10	10.0	50	50	0.1149	0.0423	0.0441	0.0745	0.0019	0.0033
20	0.5	5	30	0.4910	0.1158	0.0684	0.4418	0.0511	0.0059
20	0.5	5	50	0.4872	0.1075	0.0627	0.4429	0.0475	0.0015
20	0.5	50	30	0.6334	0.1239	0.0679	0.5850	0.0564	0.0025
20	0.5	50	50	0.6388	0.1182	0.0646	0.5998	0.0539	0.0009
20	10.0	5	30	0.5058	0.1587	0.1723	0.4736	0.1200	0.1492
20	10.0	5	50	0.4994	0.1185	0.0841	0.4534	0.0594	0.0286
20	10.0	50	30	0.6544	0.1353	0.0867	0.6008	0.0682	0.0220
20	10.0	50	50	0.6415	0.1231	0.0674	0.5915	0.0579	0.0039

(b) Tensor Product Basis

$K_{true}$	$\sigma^2$	$N$	$n_d$	$m_d$ (model d.o.f.)					
				7 (343)	8 (512)	9 (729)	11 (1,331)	12 (1,728)	13 (2,197)
10	0.5	5	30	1.1409	0.9520	0.9096	0.5327	0.4817	0.2136
10	0.5	5	50	1.1251	0.9326	0.8870	0.5067	0.4581	0.1823
10	0.5	50	30	1.1457	0.9556	0.9130	0.5338	0.4840	0.2134
10	0.5	50	50	1.1170	0.9251	0.8789	0.5020	0.4516	0.1832
10	10.0	5	30	1.1579	1.0224	1.0136	0.7705	0.7559	0.6051
10	10.0	5	50	1.1476	0.9677	0.9300	0.5822	0.5492	0.3027
10	10.0	50	30	1.1822	1.0465	1.0369	0.7861	0.7721	0.6109
10	10.0	50	50	1.1518	0.9679	0.9334	0.5857	0.5517	0.3036
20	0.5	5	30	1.8024	1.6254	1.4738	0.9819	0.7065	0.3806
20	0.5	5	50	1.7445	1.5693	1.4194	0.9342	0.6623	0.3464
20	0.5	50	30	1.8352	1.6530	1.4973	1.0030	0.7218	0.3842
20	0.5	50	50	1.8207	1.6349	1.4739	0.9748	0.6911	0.3580
20	10.0	5	30	1.8076	1.6757	1.5688	1.2221	1.0375	0.8092
20	10.0	5	50	1.8592	1.6807	1.5290	1.0597	0.7971	0.4817
20	10.0	50	30	1.9789	1.8289	1.7073	1.3210	1.1113	0.8472
20	10.0	50	50	1.8527	1.6765	1.5280	1.0560	0.7946	0.4833

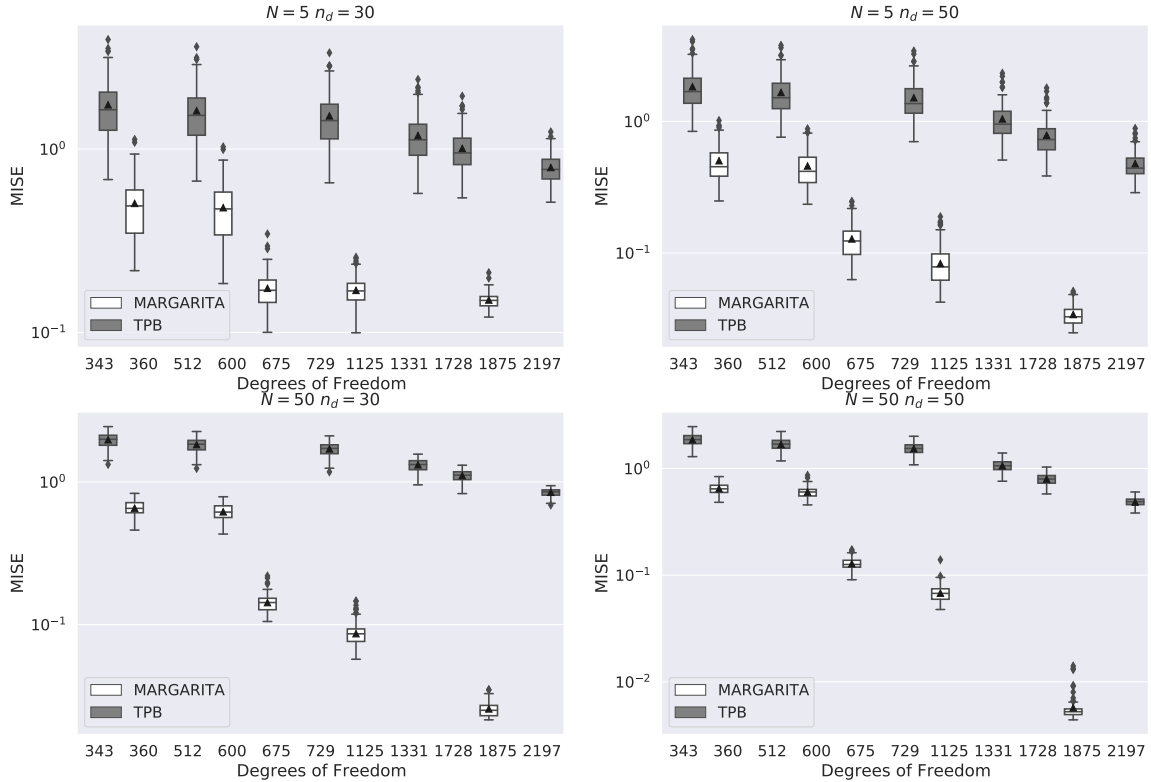


**Figure S3:** Comparison of the fit performance measured by MISE between the TPB estimated by the sandwich smoother (gray) and MARGARITA (white) as a function of the total number of degrees of freedom. For each panel  $K_t = 20$  and  $\sigma^2 = 10$ . The Y-axis is plotted on log-scale for clarity.

## S5.2 MargFPCA and Two-Stage FPCA Analysis

The eigenfunctions determining a non-stationary, non-separable anisotropic covariance function  $C(\mathbf{x}, \mathbf{y})$  over  $\mathcal{M}$  are defined as follows. Denote the eigen-decomposition of the pairwise  $\mathbb{L}^2$  inner product matrix of the tensor product basis system  $\mathbf{J}_{\phi_1 \otimes \phi_2} = \mathbf{P}\mathbf{T}\mathbf{P}'$ . The collection of  $m_1 m_2$  orthonormal eigenfunctions are defined according to  $\boldsymbol{\psi} = \mathbf{\Gamma}^{-1/2} \mathbf{P}' \text{vec}(\phi_1 \otimes \phi_2)$ . The eigenvalue corresponding to the  $k$ th eigenfunction is given by an exponential decay model  $\rho_k = \exp(-0.5k)$ . Realizations of the random function  $U_i \sim U$  are simulated using a Gaussian process assumption and then evaluated on an equispaced  $200 \times 200$  grid on  $\mathcal{M}$ .  $\phi_1$  and  $\phi_2$  are used as the marginal basis for fitting and are taken to be equispaced cubic b-splines with  $m_1 = 10$  and  $m_2 = 8$ . Note that these marginal ranks can be consistently

**Table S2:** Relative difference in moMISE for FCP-TPA and MARGARITA for marginal ranks 15 and 25 and  $K_{fit} = 8, 15, 25$ . Positive values indicate lower moMISE for MARGARITA. A grid search to select  $\lambda_d$  was performed for each fit and the results from the optimal value are reported. The entry in bold face indicates the **only case** that FCP-TPA outperformed MARGARITA.

$K_{true}$	$\sigma^2$	$N$	$n_d$	$K_{fit} = 15$			$K_{fit} = 25$		
				$m_d$					
				8	15	25	8	15	25
10	0.5	5	30	0.2113	0.2506	0.1738	0.3062	0.7949	0.7160
10	0.5	5	50	0.2544	0.2433	0.1534	0.3634	0.9328	0.8518
10	0.5	50	30	0.2062	0.2118	0.1555	0.2323	0.9228	0.8734
10	0.5	50	50	0.1597	0.1850	0.1167	0.2954	0.9757	0.9437
10	10.0	5	30	0.3684	0.2533	<b>-0.0770</b>	0.4413	0.4426	0.4895
10	10.0	5	50	0.3086	0.3824	0.2120	0.4409	0.6580	0.4486
10	10.0	50	30	0.3487	0.3509	0.1540	0.3529	0.6836	0.5607
10	10.0	50	50	0.2080	0.3300	0.2446	0.3079	0.7229	0.7629
20	0.5	5	30	0.0946	0.4304	0.4429	0.1152	0.6157	0.8706
20	0.5	5	50	0.1139	0.4149	0.4505	0.1243	0.6088	0.9428
20	0.5	50	30	0.0708	0.4452	0.4624	0.0743	0.6107	0.9699
20	0.5	50	50	0.0835	0.4274	0.4554	0.0880	0.6092	0.9816
20	10.0	5	30	0.1235	0.4651	0.3642	0.1385	0.5306	0.6020
20	10.0	5	50	0.1329	0.4600	0.5117	0.1382	0.5928	0.7476
20	10.0	50	30	0.0954	0.4489	0.5313	0.0753	0.5856	0.8161
20	10.0	50	50	0.0915	0.4349	0.5089	0.0983	0.6155	0.9299

identified via our rank selection procedure (see the bottom panel of Figure S1).

Table S3 shows the results of the simulation study in Section 5.2 for additional training sample sizes and ranks. The interpretation of the results echo those in the main text. Table S4 shows the performance of the proposed two-stage FPCA procedure for estimating the first three eigenfunctions. The estimation performance is quantified using the angular error:  $AE(\hat{\psi}_i) := 1 - |\langle \psi_i, \hat{\psi}_i \rangle_{\mathbb{L}^2(\mathcal{M})}|$ . As the eigenfunctions are unit norm, the  $AE(\hat{\psi}_i) \in$

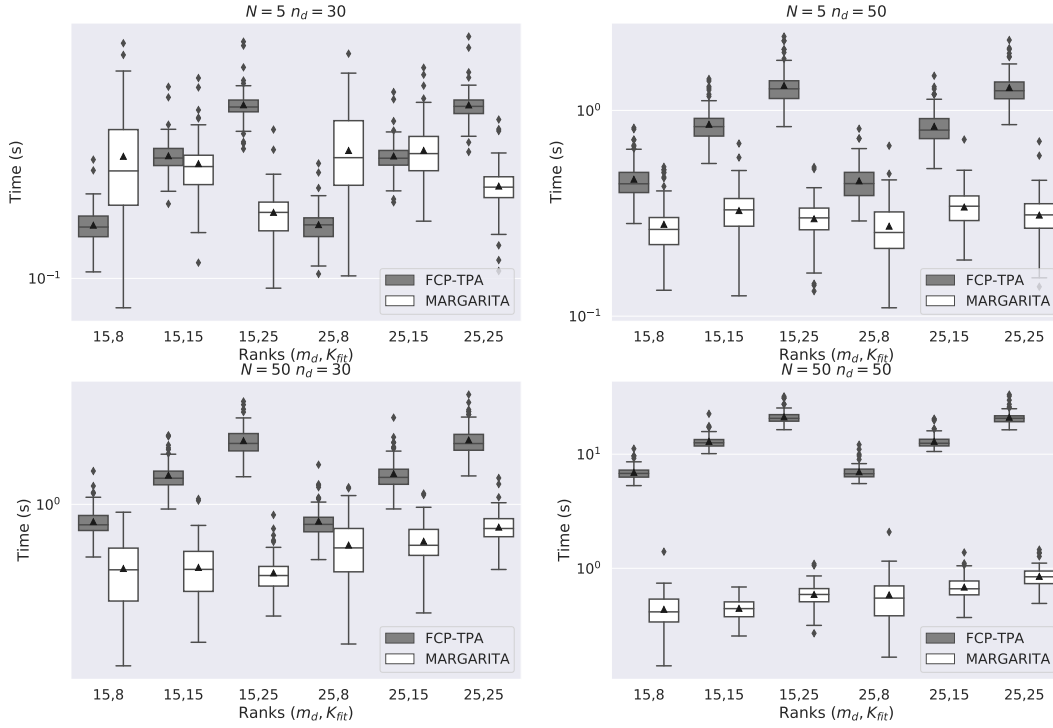


**Figure S4:** Computational time comparison between FCP-TPA and MARGARITA. The Y-axis is plotted on log-scale for clarity.

$[0, 1]$ , with 0 indicating perfect recovery and 1 indicating orthogonality. As desired, we see that the  $AE$  converging to 0 as  $N$  increases. Figure S5 shows the first three eigenfunctions (right column) and estimates from the two stage FPCA for  $N_{train} = 100$  (left column). Notice that the eigenfunctions are extremely high frequency, making this a challenging estimation problem. Despite this, the fits are nearly visually identical.

## S6 TBI Data Description and Preprocessing

All subjects in our study were referred to the University of Rochester Medical Imaging Center and imaged on the same 3T MRI scanner. Study inclusion criteria included history of concussion, while exclusion criteria included dental braces, prior brain surgery, ventricular shunt, skull fractures, or other standard contraindications for MR imaging. Diagnosis of concussion was made by neurologists, physical medicine and rehabilitation physicians, and sports medicine physicians. The control group consisted of young athletes with no history of

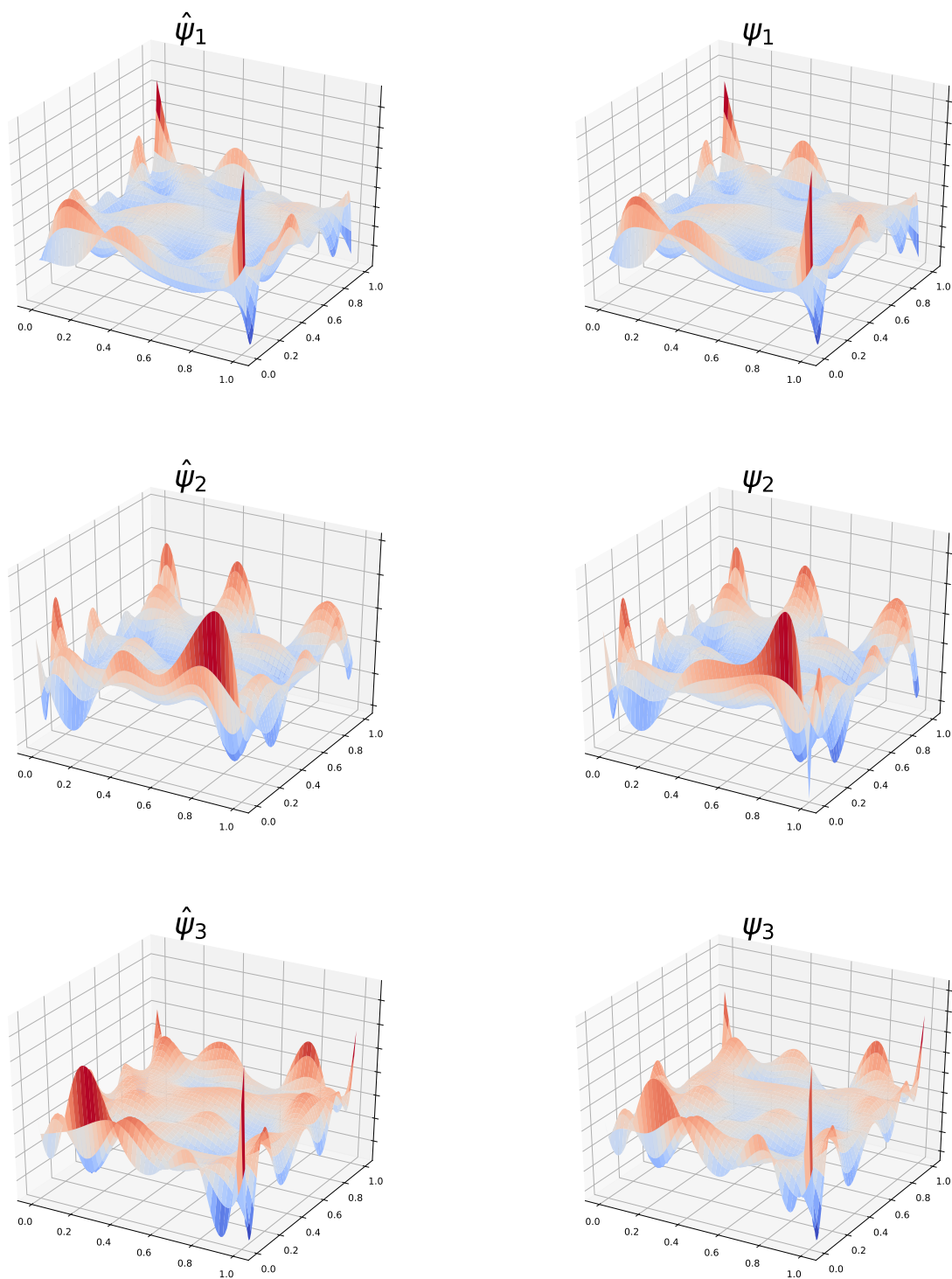


**Figure S5:** First three true eigenfunctions (right column) and their estimates using the two-stage FPCA with  $N = 100$  (left column).

**Table S3:** Monte Carlo average MISE for representing a new realization for both MARGARITA and MargFPCA, for a variety of ranks and training sample sizes.

$N_{train}$	MARGARITA				MargFPCA			
	10	20	50	100	10	20	50	100
5	1.5582	1.4204	1.3652	1.3607	2.2583	2.1277	2.1387	2.1317
10	0.8247	0.7333	0.6373	0.6104	1.9119	1.8598	1.8380	1.8800
15	0.5177	0.3554	0.3037	0.3009	1.6870	1.6224	1.5539	1.6279
20	0.3230	0.1904	0.1443	0.1324	1.4540	1.4180	1.4030	1.3785
30	0.1205	0.0535	0.0319	0.0288	1.0688	1.0780	1.0772	1.0796

$N_{train}$	20	50	100
$\psi_1$	$0.2248 \pm 0.0566$	$0.0929 \pm 0.0231$	$0.0341 \pm 0.0099$
$\psi_2$	$0.3401 \pm 0.0530$	$0.1677 \pm 0.0306$	$0.0751 \pm 0.0150$
$\psi_3$	$0.3898 \pm 0.0537$	$0.1861 \pm 0.0387$	$0.0842 \pm 0.0153$

**Table S4:** Average angular distance with standard errors for the two stage eigenfunction estimates.

concussion. The University Institutional Review Board approved this retrospective study. All MRI examinations were reviewed by an experienced neuroradiologist for any artifacts that might affect the quality of the study, as well as for the presence of recent or remote intracranial hemorrhage, signal abnormalities in the brain, hydrocephalus, congenital or developmental anomalies.

The diffusion MRI data was collected on a single 3T scanner using a 20-channel head coil (Siemens Skyra, Erlangen, Germany). Diffusion imaging was performed with a b-value of  $1000 \frac{s}{mm^2}$ , using 64 diffusion-encoding directions. In addition, a  $b = 0 \frac{s}{mm^2}$  image was collected for signal normalization. Additional dMRI parameters included:  $FOV = 256 \times 256mm$ , number of slices = 70, image resolution =  $2 \times 2 \times 2mm^3$ ,  $TR/TE = 9000/88ms$ , Generalized autocalibrating partially parallel acquisition (GRAPPA) factor = 2. Acquisition of dMRI data took 10 minutes and 14 seconds. A Gradient-recalled

echo (GRE) sequence was also collected with  $TEs = 4.92, 7.38ms$  at the same resolution of the dMRI to correct for susceptibility-induced distortion effects. A diffusion tensor model (DTI) was fit to each subject's diffusion data and used to compute the per-voxel FA. Registration of the FA images to the ICBM 2009c Nonlinear Symmetric 1mm template (Fonov et al., 2009) was then performed using the popular ANTS software (Avants et al., 2009). The domain of analysis was constrained to be the convex hull of a rectangular  $115 \times 140 \times 120$  voxel grid in the template space covering the white matter, i.e. the raw data tensor  $\mathcal{Y} \in \mathbb{R}^{115 \times 140 \times 120 \times 50}$ . A white matter mask was also applied to the aligned data.